Reprinted from Journal of the Optical Society of America B, Vol. 2, page 1155, July 1985

Room-temperature excitonic nonlinear-optical effects in semiconductor quantum-well structures

D. S. Chemla and D. A. B. Miller

AT&T Bell Laboratories, Holmdel, New Jersey 07733

Received March 1, 1985; accepted March 27, 1985

We review the nonlinear-optical effects observed at room temperature in semiconductor quantum-well structures photoexcited near the band gap. A comprehensive discussion of optical transitions in these microstructures is given, including excitonic effects and the specific features of room-temperature exciton resonances. Experimental investigations using continuous-wave, picosecond-, and femtosecond-laser sources are presented. They show extremely efficient nonlinear processes. In the case of excitations that are long compared with the exciton-ionization time, the induced changes in absorption and refraction do not depend on the wavelength or on the duration of excitation. These changes depend only on the density of absorbed photons and are interpreted in terms of electron–hole plasma screening and band filling. In contrast, for ultrashort excitation, nonlinear processes depend critically on the excitation wavelength. The selective generation of excitons is found to produce effects larger than a plasma of the same density. This unexpected result is shown to arise from the low temperature of the exciton gas before it interacts with the lattice and from the decrease of screening that is the reduced dimensionality of quantum-well structures.

1. INTRODUCTION

Excitonic effects in semiconductors have been the subject of intense research for several decades.[1] Recently they have been found to play an important role in the optical transitions near the fundamental absorption edge of the first man-made semiconductor microstructures, superlattices (SL's) and quantum-well structures (QWS's).[2] These artificial media consist of ultrathin layers of semiconductors (e.g., 100 Å thick), with different compositions, grown alternately one on the other. Advanced crystal-growth techniques[3] are now able to manufacture very-high-quality SL's and QWS's with atomically smooth layer interfaces and well-controlled compositions. Since the band structure depends critically on the composition, in these microstructures it is modulated in the direction normal to the layers, inducing highly anistropic electronic and optical properties. Along the plane of the layers, the band structure is not too different from that of the parent compounds. Conversely, in the direction normal to the layers, the abrupt composition changes produce discontinuities at various points in the Brillouin zone and result in qualitative modifications of the electronic state. Three categories of states are encountered, depending on the magnitude of the band-gap discontinuities and of the layer thicknesses: (1) states almost perfectly confined in the low-gap layers; (2) states mostly confined in the low-gap layers with, however, some interaction with their immediately neighboring layers; and (3) delocalized states with charge density modulated along the normal to the layers. Accordingly, SL's and QWS's can sustain quasi-two-dimensional[4] and/or extended excitons.[5] The present report is mostly concerned with the lowest-energy, well-confined states found in QWS's.

In this paper we review the nonlinear optical properties of QWS's at room temperature. In Section 2 we analyze the nature of the electronic states that participate in the near-band-edge optical transitions; we present a comprehensive comparison of two-dimensional (2-D), quasi-two-dimensional, and three-dimensional (3-D) excitons, and, finally, we discuss the behavior of excitons at room temperature. In Section 3 we review the nonlinear-optical effects induced by photogeneration of an exciton gas and an electron–hole (e–h) plasma. An effort is made to simplify the semantics and to give physical interpretations of the dominant mechanisms, even if some generality is sacrificed. In Section 4 we describe our experimental studies and their interpretations. This section is divided into two parts. In Subsection 4.A we review experiments in which excitations long compared with the mean time for exciton thermal ionization are used. In this case absorptive and refractive nonlinearities are found to be insensitive to the wavelength or to the duration of excitation, being sensitive instead only to the created e–h-pair density. The changes of optical properties are shown to arise from e–h-plasma effects and are well interpreted by theories based on plasma screening. In Subsection 4.B we present and discuss recent experiments with ultrashort laser sources. Such brief excitations are able to resolve the exciton ionization in real time. These measurements have also revealed that, contrary to some previous expectations, *excitons can produce changes of the optical spectra that are larger than those induced by an equal density of free-e–h pairs.* We analyze in detail the phase-space filling and the screening resulting from both species, and we present an interpretation of our observations in terms of the difference in temperature between (1) the exciton gas generated by ultrashort pulses and (2) the plasma that originates from exciton ionization or that is directly created in the continuum. The effect of the reduced dimensionality of the QWS on the relative strength of phase-space filling and screening is also discussed. Finally, some trends for future work are discussed in the conclusion.

0740-3224/85/071155-19$02.00

2. LINEAR ABSORPTION IN QUANTUM-WELL STRUCTURES

A. Single-Particle States in Thin Semiconductor Layers

In this section we examine the structure of single-particle (i.e., electron or hole) states in ultrathin semiconductor layers and discuss the optical transitions between these states. For the moment we will neglect the Coulomb interaction between electron and hole; we will return to these excitonic effects in Section 3.

The simplest starting point for the theory of the single-particle states is the effective-mass approximation (EMA), and this is the only approach that we will consider here. In the EMA it is normally presumed that the variations in potential other than the underlying periodic potential of the unit cell are slow compared with the unit-cell size; the diffraction of the particle through the lattice gives the particle its effective mass, and the other slowly varying potentials in the structure are only weak perturbations. However, it is worth noting in the present case that the interfaces among the layers in the QWS's and the SL's can be extremely abrupt (of the order of one atomic layer), and it is therefore surprising that the EMA works as well as it does. In using the EMA, we simply describe the single-particle states of ultrathin semiconductor layers using the band-structure parameters of the bulk crystal. The most obvious consequence of this is that, for thin layers, the motion of electrons and holes is quantized in the direction perpendicular to the plane of the layers. In addition, the layered structure has different symmetry from the bulk material; this has important consequences for the behavior of the particles even when they are moving parallel to the plane of the layers. In particular, the hole masses change character; paradoxically, the confinement actually changes the masses of the holes for the motion *parallel* to the layers. New selection rules also appear for optical transitions. We discuss both of these phenomena below.

Let us first consider a crude model that has the advantage of simplicity and exhibits most of the important features of the real case. This is the ideal case of a single layer of semiconductor bound by infinitely high potential barriers and whose bands in the bulk are parabolic and nondegenerate. We choose the z axis along the normal to the layers. In the plane of the layer the electrons and the holes can move freely according to the usual dispersion law

$$E_c(k) = E_g + \frac{\hbar^2}{2m_e}(k_x^2 + k_y^2), \tag{2.1a}$$

$$E_v(k) = -\frac{\hbar^2}{2m_h}(k_x^2 + k_y^2). \tag{2.1b}$$

However, in the direction perpendicular to the layers, the abrupt potential discontinuities completely confine the particles in the layer. The amplitude of the envelope wave functions must vanish at the interfaces, and consequently the wave functions can be written as

$$\zeta_j^{\infty}(z) = \left(\frac{2}{L_z}\right)^{1/2} \sin\left(j\pi \frac{z}{L_z}\right) \tag{2.2a}$$

for both particles. These wave functions form a complete orthogonal basis. In this equation L_z is the layer thickness and $(j-1) = 0, 1, 2, \ldots$ is the number of nodes of the wave function. Accordingly the eigenenergies from this quantization along z are given by

$$E_j^{\infty} = \frac{\hbar^2}{2m_{e,h}}(j\pi/L_z)^2. \tag{2.3}$$

Note that they depend on the (effective) mass of the particle. Consequently, the energy-band structure of the system consists of an infinite series of 2-D conduction and valence subbands (see Fig. 1). Note that, in all the systems that we will discuss in this paper, the conduction- and the valence-band potential wells both occur in the same material, so that electrons and holes are both confined within the same material layer. In this approximation the joint density of states that governs the optical transitions forms a series of step functions

$$g_{2D}(E) = \frac{\mu}{\pi\hbar^2}\theta(E - E_{je}^{\infty} - E_{jh}^{\infty}), \tag{2.4}$$

where μ is the e–h reduced mass $\mu^{-1} = m_e^{-1} + m_h^{-1}$. The absorption spectrum is the superposition of steps starting at $\Delta E = E_{je}^{\infty} - E_{jh}^{\infty}$ with the strict selection rule $\Delta j = j_e - j_h = 0$ imposed by the orthogonality of the conduction and the valence envelope functions.

A more realistic way to model a real semiconductor heterojunction is to use finite potential discontinuities at the interfaces with different potential discontinuities in the conduction and the valence bands. Again, the particles are free in the plane of the layer with the same dispersion law [Eqs. (2.1)]. The envelope wave functions along the normal now have a sinusoidal dependence in the layer and exponential tails in the barrier regions.[6] The boundary conditions that give the eigenergies are that the envelope wave functions and the probability current must be continuous at the interface[7]:

$$\zeta_j(z) \propto \begin{cases} \sin(q_j^{w} z) & \text{inside the well} \\ \exp(-q_j^{B} z) & \text{outside the well} \end{cases}. \tag{2.2b}$$

The eigenenergy spectrum in each band now consists of a finite number of bound states and a continuum (see Fig. 1). The energies depend on the effective masses both in the well and in the barrier region. For example, when the discontinuities are the same on either side of the well, the bound-state energies are solutions of

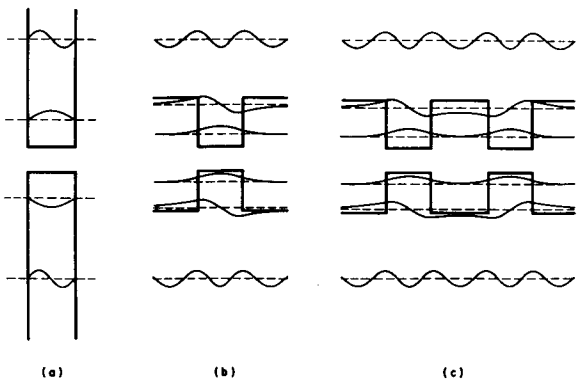

Fig. 1. Band structure of a layered microstructure in real space. (a) Single quantum well with infinite depth, (b) single quantum well with finite depth, (c) MQWS with finite depth close enough to allow significant coupling among wells. (b) and (c) show two bound states and a continuum resonance in each band.

$$\sqrt{\epsilon_j} \times \left[\frac{\cot an\left(\frac{\pi}{2}\sqrt{\epsilon_j}\right)}{\tan\left(\frac{\pi}{2}\sqrt{\epsilon_j}\right)} \right] = \frac{m_w}{m_B}(v - \epsilon_j)^{1/2}, \quad (2.5)$$

where $\epsilon_j = E_j/E_1^{\infty}$ and $v = V_{e,h}/E_1^{\infty}$ are the normalized energies and the potential discontinuities, respectively, and m_w and m_B are the effective masses in the well and in the barrier region, respectively. There is always at least one bound state. The wave functions of the low-lying states are well confined with little penetration in the barrier region. As the energy increases, the exponential tails extend more and more. The bound-state envelope wave functions in the conduction and the valence subbands are no longer orthogonal, although they do still have the same symmetry. The optical transitions are still given by steplike joint density of states, although there are some differences compared with the infinite-well case. The transitions corresponding to $\Delta j = j_e - j_h = 2p + 1$ are still forbidden because of the symmetry of the system, but those with $\Delta j = 2p$ ($p \neq 0$) are now allowed, although they are weak because of the small overlaps. The states with $E_j > V$ are delocalized and form a continuum[8]; however, there are resonances in this continuum when the normal component of their wave vector is an integer multiple of $1/L_z$. Such continuum resonances have recently been observed.[5]

The band discontinuities ΔE_c and ΔE_v are particularly important material parameters in determining the confinement. These quantities are difficult to evaluate theoretically and experimentally. For the GaAs–AlGaAs system, recent measurements using microstructures whose energy spectrum is particularly sensitive to these band parameters have given $\Delta E_c = 0.57\Delta E_g$ (Refs. 9 and 10), where ΔE_g is the difference in band gap between the well and the barrier materials. In the case of the less-well-investigated GaInAs–AlInAs system, it has been found that $\Delta E_c = 0.6\Delta E_g$.[11,12]

Two types of multiple-layer systems are of interest; multiple-quantum-well structures (MQWS's) and SL's. Strictly, any (infinite) periodic set of layers can be referred to as a superlattice. However, it is useful to make a practical distinction between those systems whose physical behavior relies on this superperiodicity and those that merely rely on confinement within a given layer. The former we will refer to as SL's, and the latter we will call MQWS's. The distinction between MQWS's and SL's depend on the relative magnitude of the barrier-layer thickness L_b and of the wave-function penetration depth in these layers L_p; let us note in passing that this distinction thus depends on which bound state is considered. In MQWS's, $L_b \gg L_p$, the wave functions in adjacent wells do not overlap, and most of the physical properties are those of a set of independent wells. Many of the properties of MQWS's can be observed with only one quantum well, and most of the physics is not really restricted to "multiple-" quantum-well structures. Although MQWS's are often grown as periodic arrays of layers, their physical properties would not change if the thickness of the barriers were different between each well layer, as long as the barriers were sufficiently thick that the wave function did not penetrate between wells. Conversely, in SL's, $L_b < L_p$; then because of the wave-function overlap, the particles are delocalized. The interaction among wells significantly modifies the physical properties of the system, and the presence of superperiodicity becomes important.

In this paper, we consider MQWS's made of III–V semiconductor compounds that have an approximately parabolic conduction band but rather complex valence bands. The simple approach outlined above for nondegenerate bands describes the energy structure of the electron subbands quite well. The description of the valence bands is, however, more complicated. In bulk III–V compounds, the valence bands consist of two $J = 3/2$ upper bands, which are degenerate at zone center, and a $J = 1/2$ spin–orbit split-off band. Within the EMA, the valence-band structure is well described by the so-called Luttinger Hamiltonian,[13,14] giving for the $J = 3/2$ multiplet a dispersion of the form

$$E_v(k) = Ak^4 \pm [B^2k^4 + C(k_x^2k_y^2 + k_y^2k_z^2 + k_z^2k_x^2)]^{1/2}, \quad (2.6)$$

where x, y, and z refer to the crystallographic directions and the inverse-mass band parameters are defined according to the notation of Ref. 14; these band parameters are simply related to the Luttinger parameters,[13] γ_1, γ_2, γ_3, and the free-electron mass m_0. For most of the III–V MQWS's, the growth is such that the normal to the layers z is parallel to a (001) crystallographic direction, and consequently the masses to be used in Eq. (2.3) or (2.5) to obtain the effect of the potential discontinuities on the holes are $(A \pm B) = (\gamma_1 \pm 2\gamma_2)/m_0$. Because the masses are different in these two bands, the effects of the confinement are different in both cases, and the valence-band degeneracy at $k = 0$ is therefore lifted by the confinement.[4] The upper band is the heavy-hole band; its angular momentum along z is $J_z = \pm 3/2$. The lower band is the light hole ($J_z = \pm 1/2$). This assignment has been confined by circularly polarized photoluminescence experiments.[15,16] For example, in the two compounds of interest in this paper, one has $m_{h\perp} = 0.45$ and $m_{l\perp} = 0.08$ for GaAs and $m_{h\perp} = 0.38$ and $m_{l\perp} = 0.052$ for GaInAs.

Let note that although this heavy and light notation is extensively used, it can be somewhat misleading; specifically, it does not apply to the motion in the plane of the layers in the presence of confinement, which is much more difficult to describe. An approach that has been used in the early studies is to model the effect of confinement in the same manner as that used for a uniaxial strain, because both phenomena have the same symmetry. For this symmetry, it is found that the $J_z = \pm 3/2$ and $J_z = \pm 1/2$ bands are completely decoupled in the (x, y) plane with a reversal in the ordering of the masses, i.e., in the (x, y) plane, the light hole becomes heavy and vice versa (the masses in the z direction are not affected). The masses determined by this method are $m_{h\parallel} = m_0/(\gamma_1 + \gamma_2)$ for $J_z = \pm 3/2$ and $m_{l\parallel} = m_0/(\gamma_1 - \gamma_2)$ for $J_z = \pm 1/2$. These masses imply a band crossing around $k = \pi\sqrt{2}/L_z$, which is, of course, unphysical. A more realistic approach is to include the potential discontinuities in the full Luttinger Hamiltonian[17,18]; this gives nonparabolic dispersion relations for the upper-two hole bands and quite strong interaction among their first few subbands. It is found that, although the upper-two hole bands are mixed away from zone center, at $k = 0$ they keep their $J_z = \pm 3/2$ and $J_z = \pm 1/2$ character, as predicted by the symmetry argument above. The corresponding selection rules for the optical transitions from the heavy- and light-holes band to the conduction band gives

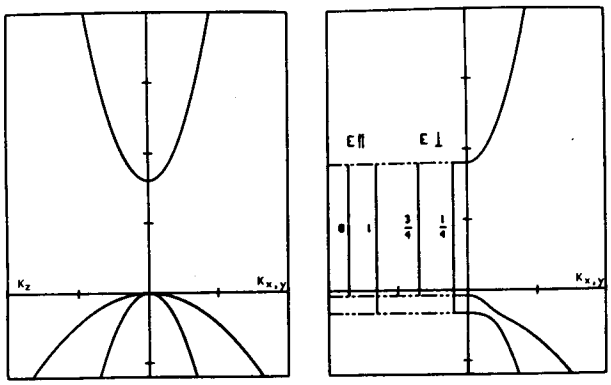

Fig. 2. Schematic of the band structure of a 3-D semiconductor (left) and of an ultrathin layer of the same material (right). The selection rules shown in the figure, for optical transitions with fields parallel and perpendicular to the normal to the layers, assume no band mixing.

relative transitions strengths of 3/4 and 1/4, respectively, for light polarized parallel to the layers, and 0 and 1, respectively, for light polarized along z (Fig. 2). This is believed to be at the origin of the polarization-dependent gain quantum-well lasers,[19–21] which can be rather well explained by models based on the EMA.[22–24]

Recently, however, polarized photoluminescence experiments have been performed in modulation-doped MQWS waveguides, and these contradict the above assignment. In these structures, light propagating along the layers can be studied, and the experiments have shown that even at $k = 0$ a significant amount of emission of light polarized parallel to z is observed. This proves that the uppermost hole subband is made up of an admixture of the $J_z = \pm 3/2$ and the $J_z = \pm 1/2$ species with a $J_z = \pm 1/2$ contribution as large as 30%.[25] At present, theories based on the EMA including excitonic effects and extrinsic symmetry-breaking mechanisms are unable to account for this phenomenon. In any case, if the light- and heavy-hole states are mixed, then the ratios of absorption strength are not those indicated in Fig. 2, the mixing reducing the contrast between the two transitions for both light polarizations.

In summary, the band-to-band optical transitions in ultrathin semiconductor layers are substantially different from those of the bulk. They form a series of steplike edges corresponding to the transitions between confined electron and hole states and also among delocalized states. The degeneracy of the $J = 3/2$ valence band is lifted by the confinement, producing two sets of transitions, and, because the symmetry of the material is altered by being grown in a layered structure, the transitions have strong-polarization selection rules.

B. Excitonic Linear Absorption in Multiple-Quantum-Well Structures

As in the case of 3-D semiconductors, the Coulomb attraction between the created electron and hole (a so-called final-state interaction) produces excitonic effects. Within the EMA the absorption coefficient of Wannier excitons is well described by Elliot's theory.[26] The pair states are expressed on the basis of single-particle states, with an envelope function that describes the pair correlation. The motion is separated into the motion of the center of gravity and the relative motion of the two particles. The motion of the center of gravity is accounted for by a plane wave and the relative motion by a wave function $U(r)$, which is the solution of an hydrogenic Schrodinger equation of the e–h relative coordinate r. In general, the absorption coefficient is related to the imaginary part of the dielectric constant by $\alpha = \omega\epsilon_2/c\eta(\omega)$, where $\epsilon = \epsilon_1 + i\epsilon_2$ and $\eta(\omega)$ is the real part of the refractive index. The absorption coefficient in a semiconductor is proportional to the probability that the created electron and hole (i.e., the electron and the hole in the final state) are in the same unit cell.[27] Regardless of whether we "turn on" the Coulomb interaction or not, this probability is given by $|U(0)|^2$ by definition. In the actual final state of electron and hole, the Coulomb interaction correlates the motion of electron and hole into hydrogenic orbits. Whether or not these orbits are bound, the result is to greatly enhance the probability of finding the electron and the hole in the same unit cell. For bound states, the sharp exciton-absorption resonances result, and for the unbound states (corresponding to hyperbolic hydrogenic orbits), we obtain the enhancement of the continuum absorption. The optical absorption is formally given by[26]

$$\alpha(\omega) = K_0 \sum_n |U_n(0)|^2 \delta(\hbar\omega - E), \tag{2.7}$$

where $K_0 = [4\pi^2 e^2/m_0 c\omega\eta(\omega)]^2 |p_{cv}|^2$, p_{cv} is the momentum operator and $U(r)$ is the envelope wave function of the correlated e–h pair in the state of energy E.[27] In the continuum part of the spectrum, the wave function depends on the continuous quantum number κ, such that $E = \hbar^2\kappa^2/2\mu$. Assuming that the wave function is slowly varying, Eq. (2.7) can be written as

$$\alpha_c(\omega) = K_0 |U_c(0)|^2 D(\omega). \tag{2.8}$$

In this equation $D(\omega)$ is the density of states corresponding to photon energy $\hbar\omega = E + E_g$.

To determine the absorption spectrum of ultrathin semiconductor layers, we need to solve the e–h Shrodinger equation in the presence of the confinement potential. Only the carrier motion is confined. Only if the static dielectric constants of the well and the barrier regions are extremely different is the functional form of the Coulomb interaction changed significantly.[28] Fortunately, in the case of III–V compounds the dielectric constants are close enough that the usual form

$$V(r) = ee'/\epsilon_0 r \tag{2.9}$$

is still valid. In this equation ϵ_0 is an effective average static dielectic constant of the two media. With this minor approximation, Elliott's theory[26] can be directly transposed to MQWS's.

In order to get an idea of the effects of reduced dimensionality, let us first consider a pure 2-D motion. In this case, and with the interaction in Eq. (2.9), the Schrödinger equation for the envelope function can be solved exactly.[29] We use as units of length and energy the 3-D Bohr radius and Rydberg, respectively, $a_0 = \epsilon_0\hbar^2/e^2\mu$ and $R_y = e^4\mu/2\epsilon_0\hbar^2$. As in three dimensions, the energy spectrum consists of a series of discrete lines and a continuum; in the continuum, the absorption is increased (compared with that of the steplike band-to-band continuum) because of the correlation. Also, as in three dimensions, only the states of zero angular momentum contribute to the absorption. The main consequence of the re-

duced dimensionality on the parameters of the hydrogenic series is to replace the principal quantum number n by $(n - 1/2)$. The energies of the bound states are now $E_n{}^{2D} = -R_y/(n - 1/2)^2$, i.e., a $1S$ ground-state binding energy four times greater than that of the 3-D ground state. The wave function of the 2-D $1S$ exciton can be written, in real and in phase space, as

$$U(r) = \left(\frac{2}{\pi}\right)^{1/2} \frac{2}{a_0} \exp\left(-\frac{2r}{a_0}\right), \tag{2.10a}$$

$$U(k) = \sqrt{2\pi}\, \frac{a_0}{[1 + (a_0 k/2)^2]^{3/2}}, \tag{2.10b}$$

respectively. The relative charge-density maximum is located at a radius $a_{2D} = a_0/4$ so that

$$E_{1S}{}^{2D} \times a_{2D} = E_{1S}{}^{3D} \times a_{3D} = \frac{e^2}{2\epsilon_0}. \tag{2.11}$$

The wave functions and the charge densities for two and three dimensions are compared in Fig. 3. The 2-D wave function is squeezed in real space, and therefore it occupies relatively a large volume of the 2-D Brillouin zone. In the continuum, the envelope wave functions are related to the confluent hypergeometric function[29] for S states; the square of its modulus at zero relative displacement is

$$|U_c(0)|^2 = 2/[1 + \exp(-2\pi\sqrt{W_{2D}})], \tag{2.12}$$

where $W_{2D} = (\hbar\omega - E_g{}^{2D})/R_y$ measures the detuning from the 2-D band gap.

It is interesting to compare the absorption coefficient per layer in two dimensions with the absorption coefficient in three dimensions. They can be written, respectively, as

$$\alpha_{2D}(\omega) = (K_0/\pi a_0{}^2)\left\{\sum_n \delta(\hbar\omega - E_g{}^{2D} + E_n{}^{2D})/(n - 1/2)^3 + 2\theta(\hbar\omega - E_g{}^{2D})/R_y[1 + \exp(-2\pi/\sqrt{W_{2D}})]\right\}, \tag{2.13a}$$

$$\alpha_{3D}(W) = (K_0/\pi a_0{}^3)\left\{\sum_n \delta(\hbar\omega - E_g{}^{3D} + E_n{}^{3D})/n^3 + 2\theta(\hbar\omega - E_g{}^{3D})/R_y[1 - \exp(-2\pi/\sqrt{W_{3D}})]\right\}, \tag{2.13b}$$

where we have used $|U_n(0)|^2 = (n - 1/2)^{-3}|U_1(0)|^2$ in two dimensions and $|U_n(0)|^2 = n^{-3}|U_1(0)|^2$ in three dimensions. The absorption strength of the exciton peaks decreases more rapidly in two dimensions than in three, i.e., $(n - 1/2)^{-3}$ versus n^{-3}. In the continuum, the correlation, which produces an almost-flat spectrum in three dimensions, gives in two dimensions a rise from the band-to-band step value far above the gap to a value twice as large at the edge. The compression of the wave function in two dimensions enhances the contrast between the $1s$ exciton and the continuum. This is clearly seen by comparing the weight of the Dirac peak (or more realistically the area under the exciton peak) A_{1S} with the absorption at the continuum edge,

$$A_{1S}{}^{2D} = 8R_y\alpha_c{}^{2D}(E_g{}^{2D}) = 2|E_{1S}{}^{2D}|\,\alpha_c{}^{2D}(E_g{}^{2D}), \tag{2.14a}$$

$$A_{1S}{}^{3D} = R_y\alpha_c{}^{3D}(E_g{}^{3D}) = |E_{1S}{}^{3D}|\,\alpha_c{}^{3D}(E_g{}^{3D}). \tag{2.14b}$$

A pictorial interpretation of Eq. (2.14b) is that the area of the exciton-absorption peak is equal to the area of a rectangle, whose base is the binding energy and whose height is the height of the continuum absorption edge. In two dimensions, the exciton-absorption area gains a factor of 4 because the binding energy is now $4R_y$, and it picks up an extra factor of 2 owing to the lowering of the dimensionality. Altogether, this results in an increased contrast between the exciton resonances and the continuum. To illustrate the exciton–continuum relative strengths in two and three dimensions, the absorption spectra are compared in Fig. 4. In order to see the excitons, we have replaced the Dirac functions by Gaussian profiles, and we have intentionally assigned a larger width to the 2-D exciton to reproduce some aspects of the broadening

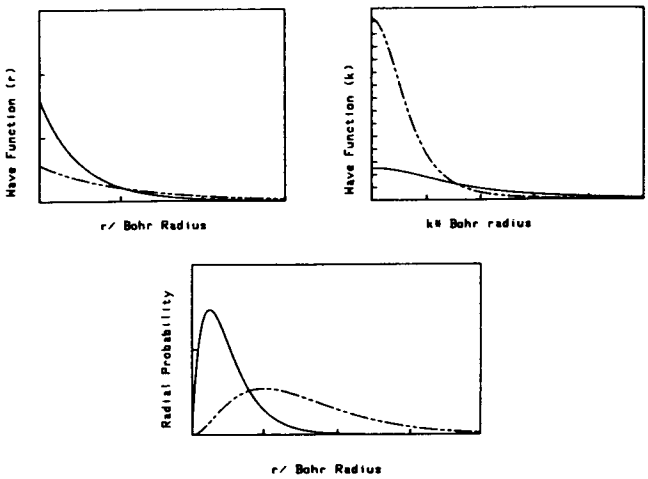

Fig. 3. Comparison of the wave functions in real space and phase space and of the radial probability distribution for 2-D (solid lines) and 3-D (dashed–solid lines) excitons.

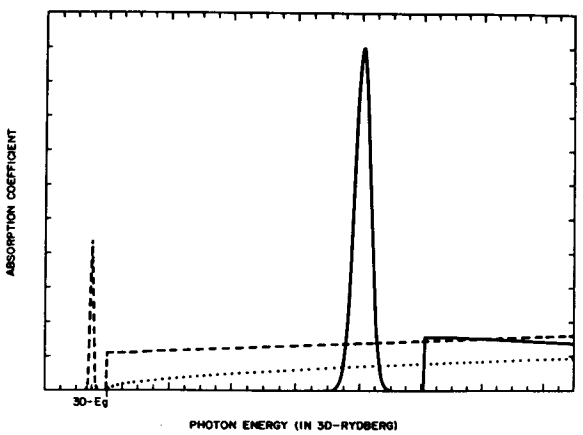

Fig. 4. Comparison of the band-edge absorption spectra in two dimensions (solid lines) and in three dimensions (dashed lines). The dotted line shows the interband absorption in the absence of excitonic enhancement in three dimensions. The theoretical infinitely narrow exciton peaks have been replaced by more-realistic Gaussian profiles. For clarity, only the $1S$ peaks have been represented. Intentionally, the 2-D exciton linewidth is chosen to be six times larger than that of the 3-D exciton to reproduce some effects of the inhomogeneous broadening of real systems. (The absolute photon energy of the 2-D absorption has been chosen arbitrarily for comparison.)

that occur in real MWQS's. For clarity in the figure, only the 1S exciton peak has been represented. The enhancement of the exciton–continuum contrast in two dimensions is striking.

Excitons in real ultrathin semiconductor layers are difficult to describe for several reasons. The layers have a finite thickness, and therefore the Coulomb interaction couples the motions in the plane and along the normal.[30] Consequently, the exciton also has finite thickness and is in neither the 3-D nor the 2-D limit. Moreover, strictly speaking, it also mixes all the electrons subbands and all the hole subbands. In addition, even if we restrict ourselves to one set of subbands, because of the complex structure of the valence subbands the hole motion in the plane cannot be described by constant masses. The exciton consists of an admixture of states with a k distribution given by a $U(k)$, whose extent can be estimated from Eq. (2.10b). Therefore, even if the light and the heavy hole were decoupled at $k = 0$, the Coulomb interaction would mix the two valence subbands. Finally, because of the penetration of the wave function in the barrier region, the differences of the masses inside and outside the well have to be accounted for. This difference is obviously important for the motion along the normal[31] and rigorously ought to be considered for the motion in the plane as well. In order to tackle the problem of the exciton in a real structure, it is necessary to introduce some approximations.

First, we assume that the light and the heavy holes are decoupled and can be described by some simple reduced masses.[32–35] Although it is possible to approach the effects of confinement as a perturbation of the 3-D wave function, the confinement is generally so severe for the conditions of practical interest (e.g., confinement of the exciton in a 100-Å layer when the 3-D diameter would be 300 Å) that perturbation methods are of limited use. Consequently variational methods are usually used for wells of finite thickness. When a perfect confinement is assumed (i.e., infinitely high barriers), various inseparable variational wave functions give a binding energy that varies smoothly between $-4R_y$ and $-R_y$ for L_z/a_0 varying from 0 to ∞. However, this result does not hold when the finite well depth is accounted for as well, e.g., $\zeta(z)$ given by Eq. (2.2b).[34,35] It is then found that, as the thickness of the layer decreases, the wave function extends more and more in the barrier material, the exciton becomes less and less confined, and the binding energy tends toward that of the 3-D exciton of the barrier compound. Therefore there is an optimum layer thickness that corresponds to a maximum binding energy; this optimum is typically found for $a_0/2 < L_z < a_0$ for which $-3R_y < E_{1S} < -2R_y$.[34,35] In the present paper we are concerned mostly with excitons of the first subband in MQWS's with rather wide and high barriers. In this case the electron and the hole are highly confined, and a simple separable wave function for the exciton is found by using the infinite-well wave functions, Eq. (2.2a), along the normal and in the plane a 2-D radial wave function, Eq. (2.10a).[36,37] The justification for this approximation is that the subband splitting is large enough compared with the Coulomb binding energy that the coupling among subbands can be neglected; this is a reasonable assumption for $0 < L_z/a_0 < 1.5$ and for large-enough potential discontinuities and can be viewed as a thin-well or a strong-confinement approximation. To account for the penetration of the wave function in the barrier medium and for the effects of finite well width on the Coulomb potential, the widths of the wells for the electron and the hole are adjusted to give the same energy as the finite-well-depth description, and the exciton radius is treated as a variational parameter. This calculation compares well with other, more complicated calculations.[36,37] The absorption coefficient as calculated using this thin-well method for finite layer thickness has the same form as that of Eq. (2.13a), with, however, a smaller binding energy. To obtain the absorption coefficient per unit volume, expressed in inverse centimeters, expression (2.13a) has to be multiplied by an extra factor $1/L_z$ that describes the finite well thickness. Overall a strong exciton–continuum contrast is still preserved, and it remains significantly larger than that in three dimensions for comparable exciton-resonance widths.

Most of the experimental work on MQWS excitons has been performed on GaAs–AlGaAs MQWS's; this material system currently offers the highest-quality structures. At low temperature, absorption spectroscopy of MQWS indeed shows the steplike structure of the absorption edge with a double exciton peak at each edge.[4,32] A striking contrast with bulk GaAs that shows the enhancement of excitonic effects in MQWS's is that intrinsic free-exciton recombination governs the luminescent emission at low temperatures, whereas, in the bulk, impurity-assisted processes dominate. Low-temperature photoluminescence experiments using circularly polarized excitation and detection have shown that the holes involved in the two excitons are mostly heavy and light in character.[15,16,32,38] Photoluminescence and excitation spectroscopoy also show that the MQWS excitons are considerably broader than those of high-quality 3-D samples. The exciton linewidth is found to increase when the layer thickness decreases. The low-temperature exciton profile has been interpreted as resulting from the inhomogeneous broadening introduced by the unavoidable fluctuations of the well thickness. In the best samples these fluctuations are found to be of the order of one atomic layer, and the size of the atomically smooth areas is of the order of 300 Å.[32,38] The effects of layer roughness on the excitons produce highly interesting properties that are due to localization, as was reviewed by Ref. 39.

The measurement of the exciton binding energy is complicated by the difficulty of determining the precise position of the continuum. Excitation spectroscopy indicated that indeed the binding energy is strongly increased by the confinement.[32] Recent magneto-optic studies seem to give even larger binding energies and are interpreted as strong evidence of hole nonparabolicity owing to valence-subband mixing.[40]

Interaction of excitons and phonons in GaAs–AlGaAs MWQS's has been investigated by resonant Raman scattering.[5,41,42] It is found that the low-lying excitons interact only with the GaAs phonons because of their confinement in the wells, whereas excitons of higher energy can interact both with GaAs and with AlGaAs phonons. In fact, excitonic resonances above the band-gap discontinuities have been observed and shown to correspond to extended excitons built from SL states.[5] The reduced symmetry of the MWQS's produces some modifications of the exciton–phonon interaction. For example, the longitudinal-optical (LO) phonons whose electric field is normal to the plane of the layers cannot change the quantum numbers in the plane but can induce changes in the quantum number describing the motion along the normal, i.e., intersubband coupling; by contrast, in the bulk material, only

intraband coupling can be seen.[41] More importantly, the Raman active modes that are seen by right-angle resonant scattering show that the modes of vibration of the GaAs layers are those of ionic thin slabs and, in particular, that they have different symmetry from the vibration modes of the bulk.[42]

C. Room-Temperature Exciton Resonances

The confinement of excitons in ultrathin layers produces several effects that are at the origin of the observation of excitonic resonances at room temperature.[43–45] First, it significantly increases the binding energy so that the resonant peaks are far from the continuum. Then it increases even more strongly the contrast between the exciton and the continuum, making the excitons easier to see. Finally, by symmetry, the confinement reduces the interaction channels between the excitons and the polar phonons that are responsible for the temperature broadening. Although the width of the exciton peak Γ is temperature broadened, it remains narrow enough to be resolved at room temperature.

It is interesting to note that these trends are quite general and should apply to a number of III–V semiconductors. From the k.p. theory it is known that the reduced mass scales with the band gap. Thus for more-infrared (i.e., narrower-band-gap) material the exciton binding energy decreases. However, since the dielectric constant does not vary drastically among these related compounds, Eq. (2.11) shows that the 3-D Bohr radius increases roughly as $1/E_{1S}$. Therefore, for the same well thickness, the confinement will produce larger compression of the exciton, and the enhancement of the binding energy resulting from the confinement will compensate to a large extent the diminution resulting from the band-gap reduction. This has been confirmed by the recent observation of room-temperature excitons in the small-gap GaInAs–AlInAs MQWS's.[12] To illustrate the effect of band-gap variation on the exciton confinement, a scale drawing of radial probability distribution of 3-D excitons in GaAs and in GaInAs is compared in Fig. 5 with the width of a 100-Å quantum well. In Fig. 6 we show the room-temperature absorption coefficient of GaAs–AlGaAs and GaInAs–AlInAs MQWS's.

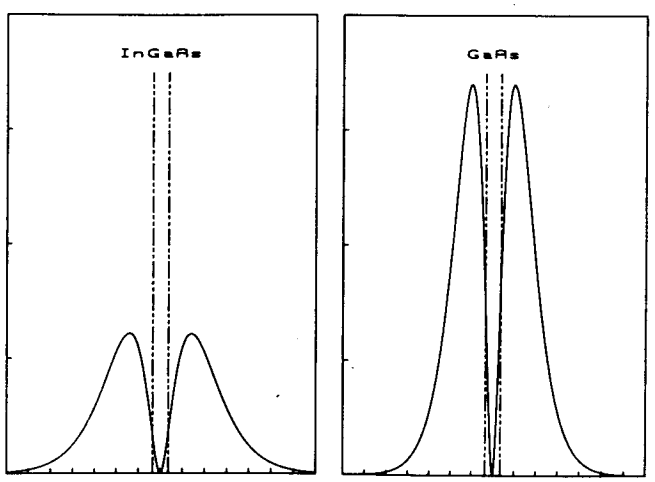

Fig. 5. Scale drawing of the 1S-exciton radial probability distribution in bulk GaAs (Eg = 1.5 eV) and GaInAs (Eg = 0.74 eV). The dashed lines represent a 100-Å-wide quantum well in which the excitons are confined in a MQWS.

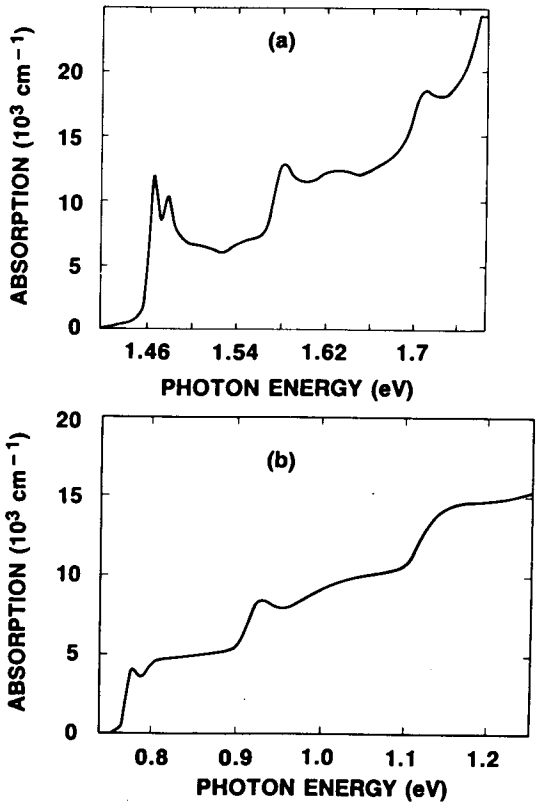

Fig. 6. Room-temperature absorption spectra of (a) a GaAs–AlGaAs and (b) a GaInAs–AlInAs MQWS's showing the strong exciton resonances and the characteristic plateaux of the 2-D continua. In both cases the quantum-well thickness is about 100 Å.

They show clearly all the features discussed above. It is worth noting that in bulk materials such strong excitonic resonances are seen only at low temperature. The observed contrast with the continuum is less pronounced than predicted, indicating that even these high-quality samples are far from being perfect. Significant improvements of the material characteristics should, however, be expected through further improvement of growth techniques.

The excitonic absorption for an optical field polarized normal to the layer is more difficult to investigate. In recent experiments, waveguide structures were used to study quantum-well absorption for light propagating along the plane.[46] Such a waveguide configuration enables polarizations both parallel and perpendicular to the layers to be used. To have an accurate control of the refractive index and of the interaction length, complex SL structures were designed that consist of a single quantum well at the center of the guiding regions. The SL material surrounding the single quantum well was designed to be substantially transparent at the quantum-well exciton-absorption wavelengths. The room-temperature absorption spectra are shown in Fig. 7. These structures exhibit a strong dichroism. For the polarization normal to the layer, the heavy-hole exciton is almost not active, and the light-hole exciton completely dominates the absorption. Within the experimental accuracy, the ratio of oscillator strengths is consistent with that indicated in Fig. 2.

The observation of excitons at room temperature has, of

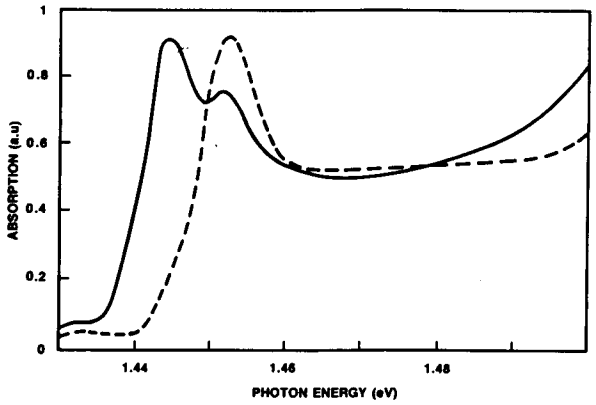

Fig. 7. Room-temperature absorption of a waveguide structure that comprises a single quantum well in the guiding regions. Light polarized parallel to the layers (solid line). Light polarized perpendicular to the layers (dashed line). A strong dichroism is observed. The light-hole exciton governs the absorption for light polarized normal to the layer; for the parallel polarization both excitons are active.

course, important implications for applications. It also corresponds to an unusual situation as far as the relative size of binding energy (E_{1S}), phonon energy ($\hbar\Omega_{LO}$), exciton linewidth (Γ), and kT are concerned. This situation is characterized by the relation

$$\hbar\Omega_{LO} > kT > E_{1S} > \Gamma. \tag{2.15}$$

Typical values of these parameters in the case of GaAs MQWS's are $\hbar\Omega_{LO} = 37$ meV, $kT = 25$ meV, $E_{1S} = 9$ meV, and $\Gamma = 3$ meV (half-width). Because $\hbar\Omega_{LO} > E_{1S}$ any collision between an LO phonon and an exciton will cause the latter to ionize. Because $kT > E_{1S}$ there is relatively a large density of thermal phonons. To illustrate this point let us note, using the well-established analogy between excitons and hydrogen atoms, that a temperature $kT \sim 2.5 \times E_{1S}$ corresponds for the hydrogen atoms to 4.5×10^5 K! Thus excitons resonantly generated at room temperature are very quickly ionized. The mean free time to LO-phonon ionization can be estimated from the temperature dependence of the peak linewidth. It is found that, in the cases of GaAs–AlGaAs[47,48] and of GaInAs–AlInAs[12] MWQS's, this temperature dependence can be expressed as

$$\Gamma = \Gamma_0 + \Gamma_{ph} \Big/ \left[\exp\left(-\frac{\hbar\Omega_{LO}}{kT}\right) - 1\right], \tag{2.16}$$

where Γ_0 accounts for the inhomogeneous broadening resulting from thickness fluctuations and agrees with the low-temperature width. The parameter Γ_{ph} describes the effect of LO phonons, which are considered as the major source of thermal broadening; it is found that $\Gamma_{ph}{}^{2D} = 5$ meV for GaAs[48] and $\Gamma_{ph}{}^{2D} = 9$ meV for GaInAs.[12] In the case of GaAs for which the exciton temperature broadening in the bulk is known, $\Gamma_{ph}{}^{3D} \sim 7$ meV[49]; comparison with MWQS's indicates that, in agreement with the previous discussion, the interaction with the LO phonons produces a somewhat smaller broadening in MQWS's. From these linear-absorption data, the mean times for ionization are found to be $T_i = 400$ fsec and $T_i = 270$ fsec, respectively, for the two MQWS's. Thus at room temperature the excitons are unstable; they live just long enough to produce the clear resonances of Fig. 6 before being ionized into an e–h plasma that in turn lasts for several nanoseconds before recombining. Thermodynamic arguments show that in the quasi-equilibrium regime, which occurs between the exciton ionization and the e–h plasma recombination, almost no excitons are present.[48] Let us note also that, owing to the fast carrier–carrier relaxation, the large difference between the LO-phonon energy and the exciton binding energy, and the rapid carrier–phonon scattering, the e–h plasma created by exciton ionization is essentially in equilibrium with the lattice at room temperature.

The most unusual situation in which excitons exist at room temperature governs the physical properties that are discussed below.

3. EXCITONIC NONLINEAR-OPTICAL EFFECTS

It is important to emphasize at the outset that the nonlinear-optical processes associated with excitons are qualitatively different from those associated with atomic systems. The reason for this is the different type of optical transition involved in each case. In the case of atomic systems, we are normally concerned with exciting some of a given number of atoms from one atomic state to another. The number of atoms is fixed, and, for example, saturation of an atomic transition will occur when we have exhausted the number of atoms available for this transition (with, of course, due allowance for stimulated emission). However, the excitonic-absorption resonances observed in the optical spectrum of a semiconductor correspond to the creation of excitons, not the excitation of existing excitons. The absorption analogous to atomic absorption for an excitonic system would be found in the far-infrared at photon energies of the order of 1–100 meV, if by some other means we had already created a population of excitons in the semiconductor. Conversely, an interesting physical analog to excitonic absorption in the case of atomic systems is the creation of positronium atoms (an electron and a positron in a hydrogenic atom) by absorption of photons in the gamma-ray region of the spectrum of free space. Whether it is possible to create further excitons in a semiconductor or positronium atoms in free space will depend on the number and the type of particles already present [e.g., excitons (positronium atoms) and free-electron and/or hole (positron) plasma]. Thus the physics of excitonic-absorption saturation (and associated nonlinear processes) is intrinsically a many-body problem, because it depends not only on the final-state interactions of electron and hole but also on the final-state interaction with all other particles in the semiconductor. As is often the case, excitons enable us to investigate the physics of hydrogenic systems under conditions not normally accessible with atomic systems.

This many-body character can be stated more formally. Excitons behave as pure bosons only in the limit of vanishing densities of bound or of free e–h pairs. As elementary excitations of the whole crystal, they are eigenstates of a large system of strongly interacting fermions, and, despite their quasi-particle character, their nonlinear-optical response cannot be accounted by a noninteracting atomlike-particle formalism.

The excitonic contribution to the dielectric constant depends on the density of excited e–h pairs in a rather subtle way. First, since they are built from a combination of single-particle states, any change in character of the single-particle state will indirectly affect the excitons. Thus Coulomb interaction and exclusion-principle effects on the single-

particle band structure (band-gap renormalization and band filling) induce changes in the optical response of excitons. Second, the nature of the combination of single-particle states that forms the exciton depends itself directly on the presence of other excited pairs, because the nature of the Coulomb attraction that binds the exciton is changed by the dynamic screening from the other excited pairs. The nature of this screening itself depends on whether these other excited pairs are themselves bound or unbound. Possible consequences of these interactions include the formation of many-exciton bound states (excitonic molecules) through Van der Walls interaction and/or quantum statistical condensation in very delicate conditions of density and weak interactions. Screening can also cause the bound-pair states to become unstable (Mott transition[50]). Finally, as excitons are composite bosons, interexciton fermion-exclusion effects also produce phase-space filling and thus saturation of the resonances.

A correct description of excitonic optical nonlinearities should treat all these processes in a self-consistent manner. This many-body problem is a difficult one for which a complete rigorous treatment is not yet available. Recently progress has been made toward a comprehensive description of near-band-gap optical nonlinearities in 3-D semiconductors.[51,52] Extension of the theory to the case of novel semiconductor microstructures such as MQWS's has just started to be investigated.[53]

The theoretical studies of near-band-gap nonlinearities are naturally expressed in the language of many-body theory, which is rather obscure to the nonspecialist. This has caused a lot of confusion, in particular among experimentalists, in regard to the interdependence of the physical mechanisms involved, their relative importance, and the hierarchy of approximations used to treat them. In this section, we present a discussion of the mechanisms that are responsible for the most important features of excitonic nonlinearities. We consider the usual case of 3-D semiconductors; quasi-2-D microstructures will be discussed in Section 5. We will attempt to keep the semantics as clear as possible. In some cases, we will simplify many-body theory results in order to give direct classical interpretations so that we can demonstrate that they are nothing but the results of rigorous treatments of simple and well-known processes. We shall consider in turn the effects of free e–h pairs and those of excitons. And since excitonic states depend both on the single-particle states and on the combinations of single-particle states that form bound pairs, we shall consider how each species is affected by the presence of photoexcited pairs.

A. Effects Due to Free-Electron–Hole Pairs

The simplest description of optical transitions in semiconductors neglects the Coulomb interaction and treats electrons and holes as ideal Fermi gases. Even such an oversimplified picture exhibits nonlinearities because of the Fermi statistics. When electrons and holes are present, the occupation of states in the conduction band and in the valence band [as described by the Fermi distributions $f_c(E) = f_e(E)$ and $f_v(E) = [1 - f_h(E)]$] reduces the interband-transmission probabilities by the factor $(1 - f_e - f_h)$. Effects associated with the inhibition of transmission probabilities are known as band-filling effects. For example, they are responsible for dynamic Burstein–Moss shifts. They are blocking mechanisms in the sense that they do not change the nature of the states involved in the transition; they block it because the initial state is empty or the final state is full. The temperature dependence of exclusion effects is simply accounted for by using the Fermi distribution functions at finite temperature; at high temperatures this can be approximated by the Boltzmann distributions when the carriers are no longer degenerate.

In the presence of an e–h plasma the Coulomb potential, expressed in reciprocal space as $V(k) = 4\pi e^2/\epsilon_0 k^2$, is screened by the longitudinal dielectric function; it can be written as

$$V_s(k, \omega) = V(k)/\epsilon_\parallel(k, \omega). \tag{3.1}$$

The calculation of $\epsilon_\parallel(k, \omega)$ is one of the central problems of many-body theory.[54] It is quite complicated because of the requirement of self-consistency and because of the long-range nature of the Coulomb interaction. In order to obtain a tractable formalism, several approximations have to be made. By treating the particle motion within the EMA and their interaction within the random-phase approximation (i.e., assuming statistical distributions of the particles), one gets the well-known Lindhard formula.[55] This expression still depends on the particle interaction and on the details of the band structure. A further simplification is to approximate the full energy spectrum of the existing particles by a single collective mode and to write for $\epsilon_\parallel(k, \omega)$

$$\epsilon_\parallel^{-1}(k, \omega) = \epsilon_0^{-1}\left[1 + \frac{\Omega_p{}^2}{(\omega + i\gamma)^2 - \Omega^2(k)}\right], \tag{3.2}$$

where ϵ_0 is the background dielectric function, Ω_p is a plasma frequency that measures the carrier density, $\Omega(k)$ is the dispersion of the single mode, and γ is a phenomenological damping constant. The parameters appearing in Eq. (3.2) have to be carefully chosen to satisfy all the sum rules.[51] This procedure is called the single-plasmon pole approximation (SPPA)[56–58]; it is valid for most situations of practical interest.

The major effect of the electrostatic interaction on the single-particle states is to change the energies (in the language of many-body theory—to renormalize the energies). Because the particles are fermions, the matrix elements of the Coulomb interaction have to be taken among antisymmetric wave functions. These matrix elements split into two parts called the correlation term and the exchange term. In the calculation of the single-particle energy shifts (the self-energy corrections), there are several ways in which the separation between correlation and exchange effects can be made. One separation method, which has the advantage of leading to simpler calculations and has a clear physical interpretation, consists of separating the shifts into a correlation-hole term and a screened-exchange term.[51] The physics behind this choice is the following: Even if the quantum nature of the particles is neglected, around an electron the classical electrostatic repulsion pushes away other particles until an effective positive charge develops; this therefore forms a correlation hole in the vicinity of the electron. This repulsion is balanced by the tendency of the particles to diffuse back into the low-density region around the electron; classically, this process is Debye screening. Because of this repulsion, the electrons tend not to get close enough for exclusion effects to become important, so that most of the physics is contained in this correlation-hole term. (In addition, it is worth noting that the exchange interaction itself produces effects similar to that of the classical electrostatic repulsions. To see this

let us assume that the classical Coulomb interaction is not active and that only the exchange interaction is active. The exchange interaction would also produce an exchange hole by repelling all the electrons in the same spin state, i.e., half as many as the classical electrostatic repulsion.) Thus when classical screening is correctly accounted for in the presence of an e–h plasma, the contribution to the self-energy owing to the screened exchange appears essentially as a small correction. The correlation-hole contribution is[51]

$$\Sigma_{CH} = \tfrac{1}{2} \sum_k [V_s(k) - V(k)]. \tag{3.3a}$$

By Fourier transforming, it can be seen to have a simple interpretation; it can be reexpressed as

$$\Sigma_{CH} = \tfrac{1}{2} \lim_{r \to 0} [V_s(r) - V(r)], \tag{3.3b}$$

which is just the classical electrostatic energy shift because of the screening. For example, if the electrostatic interaction is described by a simple statistically screened potential, $V_s(r) = -e^2/\epsilon_0 r\, e^{-r/\Lambda}$, depending on the temperature, the screening length is given by the Thomas–Fermi $[\Lambda_{TF}^{-1} = (4\pi e^2 N_F/\epsilon_0)^{1/2}]$ or the Debye $[\Lambda_D^{-1} = (4\pi N e^2/\epsilon_0 kT)^{1/2}]$ formula in the limits of low and high temperature, respectively. One finds for the self-energies

$$\Sigma_{CH} = -\frac{e^2}{2\epsilon_0 \Lambda}. \tag{3.4}$$

The slight variations of the band curvature (i.e., effective mass) that are due to the screening are usually neglected (this is called the rigid band-shift approximation). By adding the electron and the hole shifts one obtains the band-gap renormalization, $E_g(N) = E_g(0) + \Sigma_e + \Sigma_h$. An important result worth noting in passing is that, in 3-D semiconductors, the band-gap renormalization is substantially independent of the details of the band structure (e.g., effective mass) and can be described by a universal formula.[59]

In order to see how the pair states are affected by photocarriers it is necessary to incorporate self-consistently the band-filling effects, the dynamical screening of the Coulomb potential, and the dynamical shifts of the single-particle states. This is, of course, a difficult problem. However, in the limit of small densities, the effects of the e–h plasma can be treated as perturbations of the e–h-pair Wannier equation. If we write $[H_1(k, k')]$ as the perturbing Hamiltonian, the energy corrections are

$$E_n = E_n^0 + \sum_{k,k'} U_n^0(k)^* H_1(k, k') U_n^0(k'), \tag{3.5}$$

where the index 0 labels the zero-density energies and wave functions.[51] For the pair states in the continuum, one finds that, as expected, the correction to the energy is the sum of the electron and hole single-particle self-energies

$$E_c(n) = E_g^0 + \Sigma_e + \Sigma_h, \tag{3.6}$$

i.e., the continuum edge experiences the same renormalization as the band gap. For the bound-pair states, the correction to the energy is very small; it involves a sum of terms that nearly cancel each other. The physical meaning of this result is that, in a neutral bound state, the electron and the hole screen each other almost perfectly, i.e., the positive correlation hole around the electron neutralizes the negative correlation electron around the hole. An alternative way of expressing the same concept is to say that the neutral particle induces approximately no net movement of the plasma and hence no change in energy. These effects can be simply analyzed by using the statistically screened potential with the exchange and the band-filling effects neglected. From Eq. (3.4) one finds for the shift of the continuum

$$E_c(N) - E_g^0 \sim \frac{e^2}{\epsilon_0 \Lambda} = 2R_y \frac{a_0}{\Lambda}, \tag{3.7}$$

i.e., in our normal units (R_y, a_0) the shift is simply equal to twice the inverse of the screening length. On the other hand, the self-energy correction for the exciton ground state is much smaller. For our example of simple electrostatic screening, it is second order in the screening length

$$E_{1S}(N) - E_{1S}^0 = \Sigma_e + \Sigma_h - \langle U_{1S}| V_S - V |U_{1S}\rangle \sim 5R_y \left(\frac{a_0}{\Lambda}\right)^2 + 0\left(\frac{1}{\Lambda^3}\right). \tag{3.8}$$

We can now describe physically the effect of an e–h plasma on the absorption spectrum. As the density increases the position of the exciton peak hardly varies, but the continuum experiences a red shift. Consequently, the binding energy of the exciton, which is measured from the continuum, must decrease. The wave function therefore expands, causing the probability of finding the electron and the hole in the same unit cell (and consequently the integrated exciton-absorption strength), $|U(0)|^2$, to diminish. The exciton-absorption peak therefore weakens more and more, losing absorption strength. These trends can be followed by using Eqs. (2.10a) and (2.11), which show that the integrated excitonic-absorption strength (assuming a hydrogenic form) is inversely proportional to the binding energy. With increasing plasma density, this process will continue until, finally, the exciton becomes unstable, having a correlation-enhanced continuum. With further increases in plasma density, this continuum can continue to renormalize to yet lower energies. Let us note that even if the bound states are unstable (i.e., no excitons can exist), the absorption spectrum in the continuum is still enhanced by the e–h correlation. In fact, the absorption can still present peaks that are continuum resonances—precursors of the truly bound states. These resonances can be so sharp that it is easy to assign them incorrectly to the excitons.[60]

Although the shift in energy of exciton peaks with plasma density is well understood, the broadening of the peaks with increasing density is theoretically less advanced. This corresponds to the imaginary part of the self-energy of the exciton. Broadening can be clearly observed experimentally (as will be discussed below in Section 4) even at low densities, and this remains to be explained quantitatively for the quantum-well system.

B. Effects Due to Excitons

The effects of excitons on the absorption edge can be described only if interexciton interactions between electrons and holes are considered. Again in the limit of small density it is possible to separate the many-exciton Hamiltonian into a part that consists of all the intraexciton effects and a part that accounts for the interexciton ones.[51] The first part has the same form as the single-exciton Hamiltonian, and the second can be treated as a perturbation of the former. After tedious

algebra it is possible to obtain a multiexciton Wannier equation for the ground state. In this equation, it is seen that excitons produce exactly the same band-filling and exchange corrections as free carriers, provided that each exciton corresponds to an effective electron and hole distribution given by

$$f_c[E_c(k)] = f_h[E_v(k)] = \tfrac{1}{2}|U_{1S}(k)|^2. \tag{3.9}$$

This result is illuminating, and it also corresponds to the intuitive idea that an exciton occupies, in phase space, a volume equal to the volume of the Fourier transform of the real-space wave function. From Eq. (3.9), we can now understand how selective generation of excitons produces saturation of the absorption by the same exclusion process as the generation of free carriers. This is a blocking mechanism for which transitions are forbidden because states are occupied. Again the modification of the crystal states results from the Coulomb interaction.

Screening by excitons corresponds to the contribution to the longitudinal dielectric function that is due to the polarization of the bound states. It can be described by extending the usual formalism used for neutral atomic gases to the gas of excitons in the ground state. Two types of transitions can contribute, depending on when the exciton changes its relative-motion quantum number (exciton interband transitions) or if the change affects the motion of the center of gravity (exciton intraband transitions).

If only interband transitions are considered, the exciton polarizability χ_X may be calculated exactly in the same way as that of the hydrogen atom by the Kramers–Heisenberg formula, remembering that the state of lowest energy is the $1S$ state,[51,61]

$$\chi_X(\omega) = \sum_{n \neq 1S} |ez_{1S,n}|^2 \frac{2(E_{1S} - E_n)}{\hbar(\omega + i\gamma)^2 - (E_{1S} - E_n)^2}. \tag{3.10}$$

For practical purposes, this form can be simplified further by introducing the effective-gap approximation.[62] In this approach, the energy difference between the ground state and the excited states is approximated by one effective gap, Δ. Finally, the dipolar interactions among excitons are taken into account classically by the Claussius–Mossotti local-field formula. The expression of the dielectric function has the form

$$\epsilon_\parallel^{-1}(w) = \epsilon_0^{-1}\left[1 + \frac{\Omega_{PX}{}^2}{(\omega + i\gamma)^2 - \Delta^2 - \tfrac{2}{3}\Omega_{PX}{}^2}\right], \tag{3.11}$$

where $\Omega_{PX}{}^2 = 4\pi Ne^2/\epsilon_0\mu$ measures the density of excitons.[51] This expression is similar to Eq. (3.2), which gives the free-carrier screening. The screening effects of excitons are therefore qualitatively analogous to those induced by free-e–h pairs and also shift the continuum more than they shift the exciton peak. The magnitude of the screening is, however, substantially reduced because the excitonic dielectric function does not diverge at $k = 0$. The physical reason is that, if the motion of the center of gravity is neglected, to respond to an external field, excitons can only shift from the ground state to an excited state. Because of the gap between ground and excited states the transition is difficult; hence the induced polarization that screens the field is small. Comparison of the exciton screening based on this approached and the free-e–h-pair screening indicates that the neutral exciton gas is about 50 times less efficient than the charged plasma.[61]

The screening resulting from exciton-intraband transitions has been discussed recently.[63,64] This proposed new screening mechanism corresponds to a global displacement of the exciton similar to that occurring in the case of free carriers. It originates from the difference in mass of the electron and the hole. Since there is no gap in the center-of-gravity spectra, this screening would be much larger than that resulting from interband transitions. A variational calculation of the Mott transition that is due to free carriers and to intraband-exciton screening shows that at low temperature it would occur at an exciton density only 8.5 times larger than that of the plasma. Moreover, it indicates that at $T \sim 100$ K the Mott densities of free-e–h pairs or of bound pairs would be approximately equal.[64]

In summary, the effects of a resonant photogeneration of excitons are in essence qualitatively similar to those of free-e–h pairs. The screening is more atomiclike and thus is expected to be weaker, especially at low temperature. On the other hand, excitonic effects that are due to the exclusion principle are governed by the extension of the exciton wave function in the phase space and can be comparable with those seen with free carriers.

The situation in which excitons and free-e–h pairs coexist is of course much more difficult to describe, partly because excitons may ionize into free pairs. Accounting for the delicate balance of the transformation of one species into the other is necessary. A full treatment of this situation is not yet available. The difference in screening strength implies that the transitions between insulating and metallic phases are different, depending on the starting phase.[64]

The behavior sketched in this paragraph has been studied in 3-D semiconductors at low temperature by Fehrenbach *et al.*[61] They have observed that the shift of the exciton is indeed quite small compared with that of the continuum. They have concentrated their analysis on the Mott transition and shown that it occurs at higher exciton densities than free-e–h-pairs densities. However, the experimental curves presented by these authors also show a strong bleaching of the exciton peak even in the case of resonant pumping in which only exciton density and absorption coefficient exist, it can be shown that the measured absorption bleaching is in quantitative agreement with that deduced from the exciton phase-space filling.

4. ROOM-TEMPERATURE EXCITONIC NONLINEARITIES IN MULTIPLE-QUANTUM-WELL STRUCTURES

A. Continuous-Wave and Picosecond Excitation

Saturation of excitonic absorption at room temperature has been extensively studied using cw and picosecond lasers in GaAs–AlGaAs MQWS's,[43,47,48,65] and recently preliminary results have been reported for GaInAs–AlInAs MQWS's.[66]

For these long-duration excitations, the effects observed are the same whether the photon energy of the pump is resonant or nonresonant with the exciton energy, provided that only the same number of carrier pairs is created in each case. This observation is consistent with the subpicosecond thermal-phonon ionization time of the excitons at room temper-

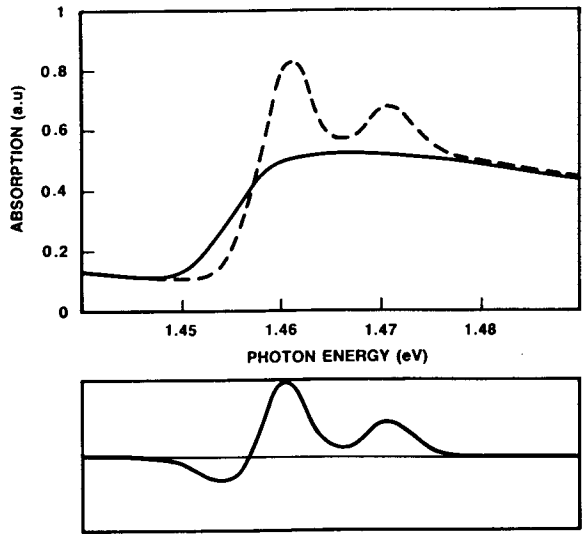

Fig. 8. Absorption spectra of a MQWS measured with tunable dye laser at low power with (solid line) and without (dashed line) the direct generation of free-e–h pairs excited in the continuum 32 meV above the heavy-hole exciton peak with a cw laser diode. The spectrum at the bottom of the figure shows the difference between the unexcited and the excited spectra.

ature deduced from the temperature dependence of the exciton linewidth. Under cw or picosecond excitation, the excitons selectively generated by resonant pumping transform in a very short time into an e–h plasma. Thus it makes no difference whether the free-e–h pairs are created directly or through the short-lived bound state. In agreement with this interpretation, it was checked that the recovery time of the absorption corresponds to the e–h-recombination lifetime, i.e., about 30 nsec. Since there is negligible actual density of excitons after about a picosecond, it seems therefore contradictory to describe the nonlinear changes in the absorption as excitonic. Note, however, that although the excitons themselves may not live very long, the possibility of creating more excitons still has a profound effect on the linear spectrum, and the nonlinear changes in the absorption spectrum can also be dominated by excitonic effects, since it can be the excitonic components of the spectrum that are changed. In essence, what is monitored in these experiments is not the density of excitons but rather the possibility of creating more, and that depends critically on the density of e–h pairs already there.

A typical example of the changes induced by an e–h plasma on the absorption spectra of a GaAs–AlGaAs MQWS's is shown in Fig. 8. In these experiments a cw laser diode operating at photon energy 35 meV above the heavy-hole exciton peak was used to generate free-e–h pairs in the continuum directly, and a weak, tunable beam from a cw dye laser was used to measure the sample transmission. The pump intensity was approximately $I = 800$ W/cm^2, generating a density of carriers $N \sim 2 \times 10^{12}$ cm^{-2} in the ~100-Å-thick GaAs quantum wells [corresponding to a density per unit volume in the well of $\tilde{N} = N/L_z$ and to an average density per unit volume $\tilde{N} = N/(L_z + L_b)$ that accounts for the thickness of the barrier as well]. At such large excitation, the two exciton peaks are completely bleached, leaving a steplike absorption edge. At the bottom of Fig. 8, a differential spectrum is shown. It is obtained by measuring directly the difference between the two spectra at the top of the figure. It is positive when the nonexcited absorption is larger than that under excitation, as, for example, at the two exciton peaks in this figure. A negative difference corresponds to an increase in absorption resulting from the pumping as seen here below the heavy-hole exciton peak. Differential spectra are highly sensitive to small changes and are used whenever accurate measurements are needed. From such measurements, it was found that the absolute change of absorption at the heavy-hole exciton varies linearly with the pump intensity up to $I \sim 300$ W/cm^2 before saturating, whereas the steplike edge was found difficult to bleach further.[48] The same behavior was observed for resonant pumping with a tunable cw dye laser; this permitted us to observe the saturation of the edge once the exciton peaks had disappeared. The intensity at which the edge saturates was found to be about 2 orders of magnitude larger than for the exciton.[47]

Semiempirical fits of the linear-absorption spectra show that they are rather well described by two Gaussian resonances and a broadened 2-D continuum.[48] In the small-signal regime, the changes in the spectrum measured by differential techniques can be accounted for by a loss of absorption strength of the exciton peaks and by broadening, with no significant shifts and no variation of the continuum contribution. At higher excitation it becomes necessary to assume displacements of the continuum and more-complicated changes of the exciton resonances. Once any excitonlike peaks have disappeared, the steplike edge shown in Fig. 8 is found to have precisely the same profile as the broadened 2-D continuum used to fit the linear absorption. The same trends are also observed in GaInAs–AlInAs MQWS's.[12]

This behavior is easily interpreted in terms of the mechanisms discussed in Section 3. As the plasma density increases, the energies of the single-particle state renormalize, causing the continuum edge to shift down in energy, whereas the exciton energies hardly change. The red shift of the continuum is accompanied by a decrease of the binding energy of the bound states. These lose absorption strength both because of the loss of e–h correlation and because of the occupancy of single-particle states that can now no longer contribute to the bound-state wave function. At large excitation, well beyond the Mott density (i.e., when the band-gap renormalization exceeds the exciton binding energy), only the 2-D-like continuum is observed. In the case shown in Fig. 8, the renormalization of the 2-D continuum is large enough to shift the new absorption edge below the lowest-energy exciton resonance. The absorption can saturate further with increasing excitation but at a smaller rate. In the intermediate regime before the peaks disappear completely, the changes in absorption are difficult to describe because bound states transform progressively into continuum resonances. In these states, the correlation between electron and hole is large enough to produce pronounced bumps in the spectra yet is not sufficient to open a binding-energy gap to produce true bound states.[60] Of course, the spectral shapes of continuum resonances are too complicated to be accounted by the simple profiles used in our semiempirical fits.

The real (i.e., refractive) part of the optical nonlinearity of GaAs–AlGaAs MQWS's was determined by simultaneously measuring absorption saturation and degenerate four-wave mixing with a tunable picosecond dye laser.[65] Analysis of the small-signal regime using variations of the semiempirical fits

and the Kramers–Kronig transformation[48] provides the complete spectra of the real and the imaginary part of the nonlinearity as defined by the relations

$$\alpha(N) = \alpha(0) - \sigma_{eh}\tilde{N}, \tag{4.1a}$$

$$\eta(N) = \eta(0) - \eta_{eh}\tilde{N}, \tag{4.1b}$$

where $\tilde{N}$ is the average carrier density per unit volume. The variations of σ_{eh} and η_{eh} versus the photon energy are presented in Fig. 9. They reproduce accurately the experimental results, as is shown in Fig. 10, where the experimental spectra of the linear absorption of the differential nonlinear absorption and of the four-wave-mixing efficiency are compared with the theoretical ones. The maximum values of the nonlinearities are very large; $\sigma_{eh} \sim 7 \times 10^{-14}$ cm^2 and $\eta_{eh} \sim 3.7 \times 10^{-19}$ cm^3. If these quantities are expressed in terms of nonlinear susceptibilities, they correspond to $\chi^{(3)} \sim 6 \times 10^{-2}$ esu, i.e., much larger than any reported in any other semiconductor. As a demonstration of the remarkable optical nonlinearity of MQWS's, degenerate four-wave-mixing experiments were performed using as sole light source a cw laser diode. In a sample 1.25 μm thick and using a pump intensity as low as 17 W/cm^2, we observed a diffraction efficiency of 0.5×10^{-4}, comparable with that usually achieved by using high peak intensities and considerably thicker samples in other materials. This represents the first reported demonstration of a cw laser-diode-induced third-order nonlinear optical process in a semiconductor. The large nonlinear cross section of excitons in MQWS's has also been utilized to mode lock semiconductor laser diodes. Stable operation showing no degradation over several months has been observed, and production of pulses as short as 1.6 psec has been reported.[67]

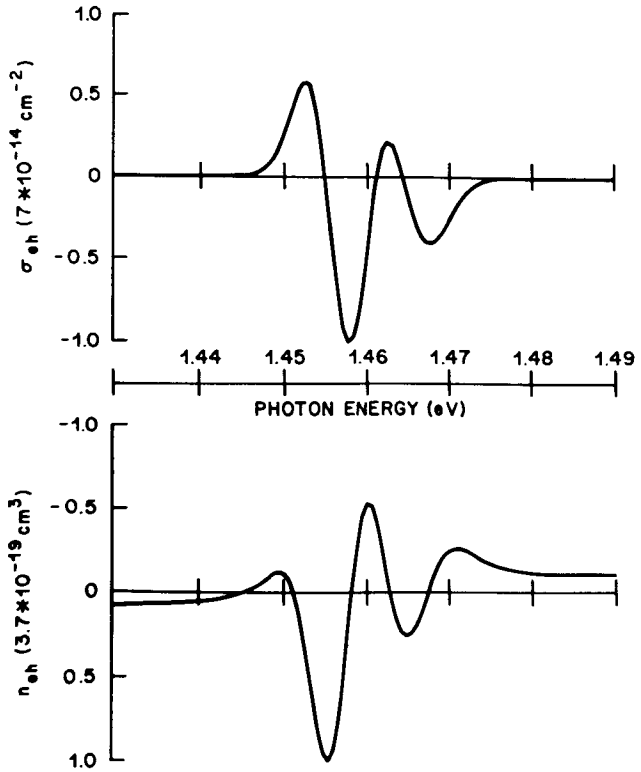

Fig. 9. Spectra of the real (σ_{eh}) and the imaginary (η_{eh}) parts of the nonlinear-optical cross section that measures the changes in absorption and in refractive index induced by one e–h pair in 100-Å GaAs quantum wells at room temperature.

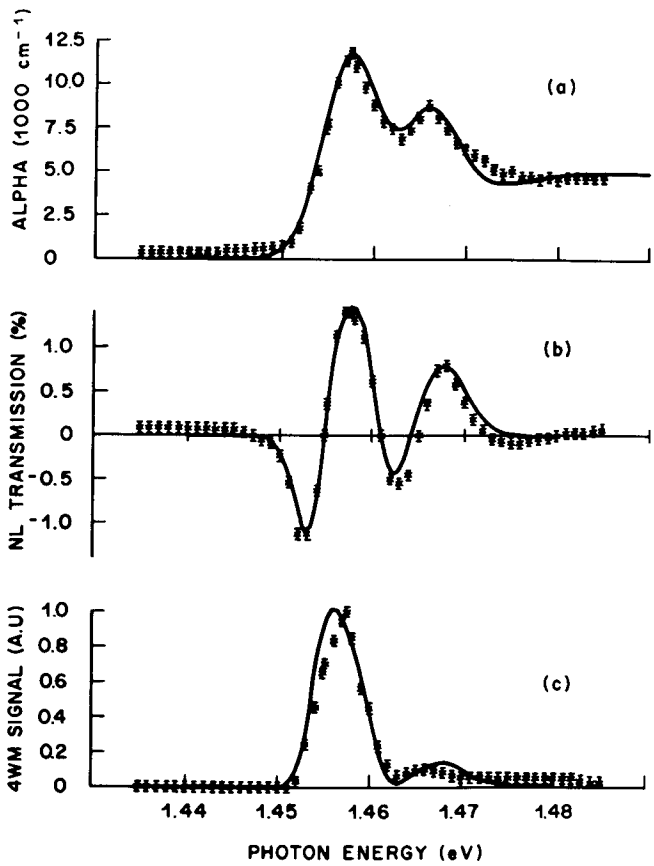

Fig. 10. Comparison of the experimental spectra (crosses) for (a) linear absorption, (b) nonlinear absorption, and (c) degenerate four-wave mixing with the theoretical spectra (solid lines) using the model discussed in the text.

Optical bistable devices based on MQWS's nonlinearities have also been operated.[68]

The magnitude of the measured nonlinearity is in quantitative agreement with a simple hard-core model of the exciton screening by an e–h plasma.[48] The model assumes that a carrier locally perturbs the MQWS's in such a way that excitons can not be generated within a small area around it. Assuming that the range of the perturbation is of the order of the exciton Bohr radius, it is found that the intensity dependence of the absorption coefficient is given by a simple Lorentzian functional form. The saturation intensity deduced from this simple model has a very intuitive interpretation. It corresponds to the intensity that should be incident upon the sample to generate one carrier per exciton area per carrier lifetime, and its value is in good agreement with experiments. Of course, such a crude model cannot describe all the details observed experimentally, and its agreement with experiment should be considered partly fortuitous.

Recently, more-elaborate many-body theory calculations have explained most of the features discussed above.[53] In this theory, the excitons are assumed to be ionized by the thermal phonons, and free-e–h-pairs effects are considered dominant. The renormalization of bound- and free-pair energies is treated in the SPPA adapted to two dimensions. As in three dimensions, the remarkable lack of shift of the exciton energy compared with the shift of the continuum is verified. The exciton Schrödinger equation, including correlation, exchange,

and room-temperature Boltzmann-distribution phase-space filling, is solved variationally by taking a 2-D 1S state as the trial function [i.e., Eq. (2.10)] and using the radius $a(\tilde{N})$ as variational parameter. To first order in the pair density, the oscillator strength of the exciton embedded in the 2-D plasma is found to be reduced by the factor $(1 - \tilde{N}/N_s)$ in which the saturation density consists of two terms, $N_s^{-1} = N_0^{-1} + N_b^{-1}$.[53] The first term describes the changes of the exciton orbital owing to correlation and exchange

$$1/N_0 = (2/\tilde{N}) \lim_{N \to 0} [1 - a(N)/a_{2D}], \qquad (4.2a)$$

and the other one describes the band-filling blocking effects

$$1/N_b = (1/\tilde{N}) \sum_k [f_e(k) + f_h(k)] \frac{|U(k)|}{|U(r=0)|}. \qquad (4.2b)$$

The theory shows a good quantitative agreement with our results, the experimental data point lying exactly between the static-screening and the dynamic-screening curves.[53] At present, the theory remains to be extended to explain the broadening of the exciton line with increasing carrier density, although some reduction of exciton lifetime (with a consequent broadening of the exciton peak) is to be expected qualitatively owing to, for example, collisions of excitons with carriers.

B. Femtosecond Studies of the Excitonic Optical Nonlinearity

All the experimental results and the interpretations discussed so far predict subpicosecond dynamics of the exciton population. Since effects induced by bound e–h pairs are quite different from those that are due to free-e–h pairs, the exciton ionization should be observable in the time dependence of the absorption spectrum after selective generation of excitons. At room temperature, the very short value of the ionization time necessitates the use of the recently developed femtosecond spectroscopic techniques.[69] To perform true selective generation of excitons, the pulse duration has to be compatible with the exciton linewidth. This condition sets an optimal pulse duration around 100 fsec for the observation of exciton ionization.

Experiments using the pump–probe configuration with a 150-fsec resolution have resolved exciton ionization in MWQS's for the first time. In addition, they have also shown unexpected results that we will now discuss.[70,71]

In these investigations, the pulses emitted by a colliding-pulse mode-locked laser were amplified to generate high-energy infrared continua 150 fsec in duration at a repetition rate of 10 Hz.[72] Narrow-band (100-Å) dielectric filters were used to select the pump-pulse wavelength from an intense continuum. Two sets of photon energies could be selected for resonant and nonresonant excitations. The resonant excitation was designed to generate primarily excitons (i.e., the pump-wavelength band overlapped the heavy-hole exciton peak), and the nonresonant excitation at a photon energy above the band-gap energy created free-e–h pairs directly. A second independent and significantly weaker broadband continuum was used to probe the absorption at various delays. An appropriate choice of neutral-density filters was used to adjust the concentration of excited e–h pairs to 7×10^{10} cm^{-2} (the same density was used in both pumping conditions) for the majority of the experiments. This rather low concentration was chosen in order to remain in the small-signal regime, where the changes in the absorption spectra are small and, in particular, the exciton peaks remain observable. The origin of time ($t = 0$) was set to correspond to the overlap of the two pulses in the sample and was defined to better than 100 fsec.

Depending on the probe delay, two distinct regimes were observed. At long times after the arrival of the pump pulses, i.e., for $t > 0.8$ psec, a quasi-equilibrium regime is established. It is characterized by two features. (1) In this regime the spectrum changes very slowly in time; (2) the changes induced in the absorption spectrum by resonant or by nonresonant pumping are indistinguishable, even when observed on the differential spectra. They are also the same as those observed with cw and picosecond excitations. In contrast, during the brief transient regime that occurs for $t < 0.8$ psec, the variations of the absorption spectrum depend strongly on the wavelength of excitation.

In the case of nonresonant pumping, the spectrum transforms progressively from the low excitation profile (dashed curve in Fig. 11) to the quasi-equilibrium profile (solid curve in Fig. 11). [The data in Fig. 11 are taken at a relatively high excitation (10^{12} cm^{-2}) for comparison with the cw spectra (Fig. 8).] The similarity between the curve obtained with femtosecond excitation and that obtained with cw excitation (Fig. 8) is striking. These high excitation data are taken at the point where nearly all traces of resonant peaks have disappeared from the spectra, and they are both well fitted with a theoretical spectrum containing only a shifted 2-D-like continuum component. This similarity between the nonresonant spectra and the cw spectra extends to low excitation as well. However, for resonant pumping the evolution of the spectrum is qualitatively different. The contrast in profile dynamics for the two types of excitation is clearly evident on the two sets of differential spectra, taken at 200-fsec intervals, that are presented in Fig. 12. On the $t = 0$ curve, it is seen that, when the heavy-hole exciton is resonantly pumped, it experiences almost instantaneously a very strong bleaching; in contrast, the $t = 0$ differential spectrum for nonresonant excitation shows only a small reduction of absorption at the heavy-hole

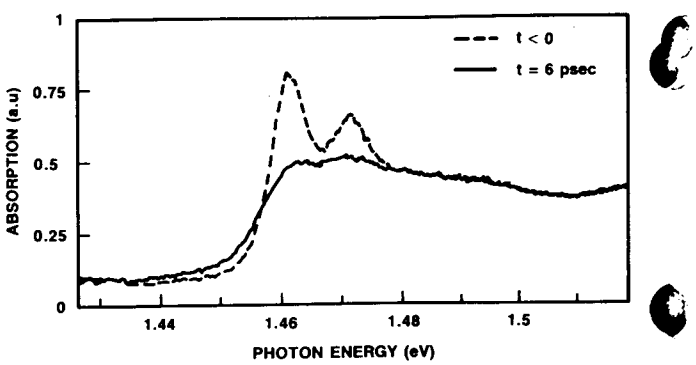

Fig. 11. Absorption spectra of a multi-quantum-well sample measured with a very weak femtosecond continuum before and 6 psec after the resonant excitation at the heavy-hole exciton peak by a 150-fsec pump pulse. The comparison with the spectra of Fig. 8 taken with cw lasers is striking. It shows that, in the quasi-equilibrium regime (that is reached 0.5 psec after the pump pulse), free carriers produce the same absorption independently of how they are created.

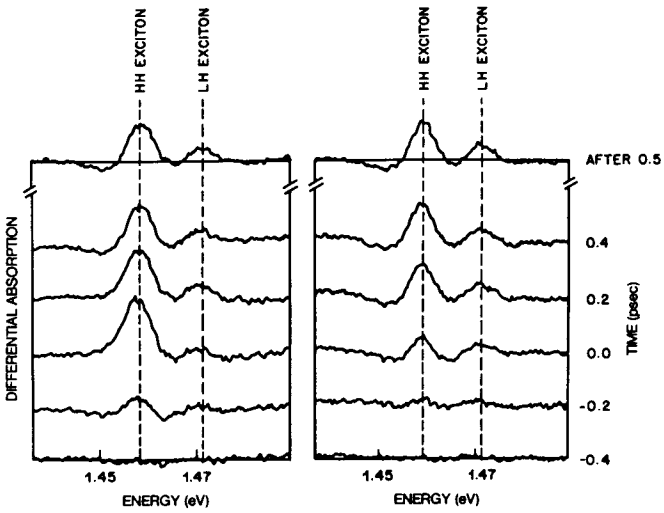

Fig. 12. Sets of different spectra taken at 200-fsec intervals for resonant (left) and nonresonant (right) excitation at the heavy-hole exciton. In the case of direct generation of free-e–h pairs, the changes in the absorption are proportional to the total number of carriers present in the sample of the arrival of the probe pulse. In the case of generation of excitons, a strong instantaneous bleaching is observed first ($t = -200$-, 0-, and 200-fsec delay), and it transforms into the change seen for nonresonant pumping at long delays as the excitons ionize.

exciton. The larger efficiency of bleaching induced by the selective generation of excitons is further supported by the comparison of the $t = -200$-fsec differential spectra. At this negative delay, the center of the probe pulse arrives on the sample before that of the pump pulse. As expected, for nonresonant excitation not much change is induced in the absorption, and the differential spectrum is almost flat. Conversely, for resonant pumping a small but clear bleaching of the heavy-hole exciton peak is already visible. This observation is interpreted as follows: At $t = -200$ fsec, the leading edge of the pump pulse starts to penetrate the sample, generating an extremely dilute population of e–h pairs. There are too few free-e–h pairs to produce noticeable changes of the absorption, yet the same density of excitons is effective enough to induce a measurable bleaching that is mostly centered at the heavy-hole exciton peak. *This proves that at short times the selective generation of excitons is much more efficient in depleting the absorption of the exciton peak than the direct excitation of free-e–h pairs.* Then, in about 0.8 psec, the absorption at the heavy-exciton peak is found to increase; however, it does not recover completely, and it settles after $t = 0.8$ psec to the same level as for nonresonant pumping when the quasi-equilibrium regime is finally established. The spectral dependence of the changes induced near the heavy-hole exciton peak also indicates different mechanisms in the two pumping cases. For resonant excitation up to about 300 fsec after the pulse center, the differential spectra are positive at the exciton peak and just below, showing that the lowest-energy transitions are blocked. Then a small negative dip develops below the peak, showing that, at these wavelengths, the absorption eventually increases under excitation. The same dip is also observed from the beginning under nonresonant pumping and corresponds well to that observed under cw excitation. This feature was interpreted as resulting from broadening of the excitonic absorption. It is interesting to note that, in contrast, the changes around the light-hole exciton are quite similar in the two cases. All the features in the differential spectra for nonresonant excitation show the progressive and smooth evolution mentioned above.

To follow the dynamics more precisely, the time variation of the amplitude of the heavy-hole exciton peak for the two pumping cases is presented in Fig. 13.[70,71] In the small-signal regime, when free-e–h pairs are directly created in the continuum, we expect the induced changes to be proportional to the carrier concentration, and indeed the dashed line in Fig. 13 follows the integral of the pump pulse well. The solid line gives the effects of the selective generation of excitons by resonant excitation. It can be fitted accurately by a model assuming the instantaneous generation of excitons with a nonlinear cross section $\sigma_X \sim 10^{-13}$ cm^2 that transform in 300 fsec into free-e–h pairs with a nonlinear cross section $\sigma_{eh} \sim 5 \times 10^{-14}$ cm^2, which then live for a very long time, i.e., several nanoseconds. The cw, picosecond, and femtosecond nonlinear cross-section measurements for free-carrier effects are in excellent agreement.

Finally, in order to verify the role of thermal phonons in the exciton-absorption dynamics, the same resonant-pumping experiment was repeated at 15 K, where the phonon density is substantially smaller. The variation of the heavy-hole exciton peak in this case is shown by the dashed–dotted curve in Fig. 13. The same instantaneous bleaching is observed, but in this case the absorption takes a very long time (13 psec) to recover.[71]

These experiments are the first to our knowledge to resolve the ionization of exciton by thermal phonons in real time. The measured ionization time $T_i = 300 \pm 100$ fsec is in excellent agreement with the value predicted from the line-shape analysis, and it corresponds quite well to the mean time for collisions between LO phonons and free carriers in GaAs.[73]

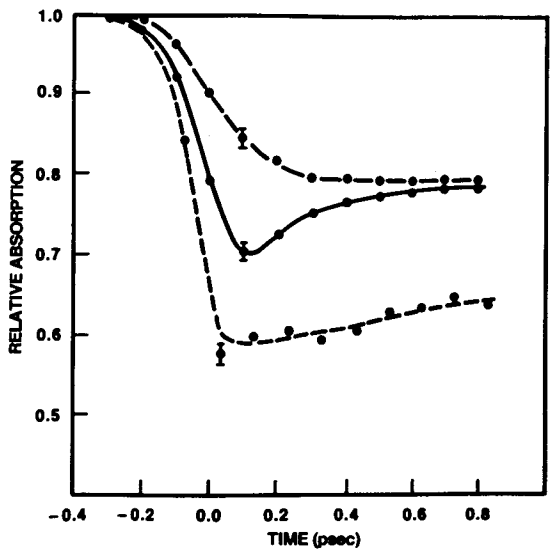

Fig. 13. Dynamics of the heavy-hole exciton-peak absorption under femtosecond excitation at room temperature for resonant pumping (solid line) and nonresonant pumping (long-dashed line) showing the exciton ionization and the stronger saturation induced at short times by excitons. The effect of density of thermal phonon on the ionization is shown by the short-dashed line, which gives the dynamics of the exciton peak under resonant pumping at a temperature of $T = 15$ K.

The results also show that the effects of excitons on the absorption spectra can be larger than those of free carriers. This surprising result is in contradiction to commonly accepted ideas and deserves some discussion.

Until now, theoretical and experimental comparisons between the optical consequences of free carriers and exciton populations have compared the effects of the two species *at the same temperature and in three dimensions.* Our work presents two novel aspects, the extremely short duration of the optical excitation and the reduced dimensionality of the samples, both of which are important in the interpretation of our results.

First, in two dimensions or in quasi-2-D systems, because the particle motion is restricted, the screening effects can be significantly smaller than in three dimensions. In the extreme 2-D limit, the screened potential of a point source falls off at large distance at a considerably slower rate than the exponential decay in three dimensions; $V_s(r) \sim e^2\Lambda_s{}^2/\epsilon_0 r_s{}^3$.[74] In that case, the screening length at high temperature is $\Lambda_s = \epsilon_0 kT/2\pi Ne^2$, and at low temperature it becomes independent of the carrier density, $\Lambda_s = \epsilon_0\hbar^2/4me^2$. The case of multilayer systems is intermediate between two and three dimensions.[75] In this case, at short distance the form of the screened potential of a point charge is complicated,[75] but it has the usual Yukawa functional form at extremely long distance, both in the plane of the layers and normal to the layers; the screening length is, however, changed: $\Lambda_s = (L_b\epsilon_0 kT/4\pi Ne^2)^{1/2}$. The appearance of the barrier-layers thickness in this expression reflects the fact that, for a point source in a layer, the screening charges of the other layers cannot approach closer than L_b, and hence the screening is partly inhibited compared with that in three dimensions. Thus, in our samples, the relative strength of the blocking and the exchange mechanisms owing to the exclusion priniciple is enhanced compared with that of electrostatic screening.

In addition, when excitons are generated selectively at the lowest-energy states of the system, for a brief moment their temperature is essentially zero. It is one of the advantages of femtosecond spectroscopy that it enables us to observe the gas of excitons *before they can interact with the thermal reservoir.* As excitons collide with LO phonons they release e–h pairs, whose energy is at least $\hbar\Omega_{LO} - E_{1S} \sim 25$ meV and which thermalize among themselves and with the lattice in a few hundred femtoseconds. Thus our experiment compares the effects of a gas of exciton at 0 K with those of a warm e–h plasma. The free-carrier band-filling effects and screening are strongly reduced by the high temperature, whereas, at short times, excitons are as efficient as they would be at very low temperature.

Let us first consider the blocking mechanisms. As was already mentioned, the generation of one exciton produces the same phase-space filling as a distribution of electrons and holes given by Eq. (3.9). If we use this distribution in Eqs. (3.2) and (4.2b) and assume a 2-D 1S wave function for the exciton, i.e., $U(k)$ given by Eq. (2.10b), a surprisingly simple expression is found for the saturation density[76]:

$$\frac{1}{N_s} = \frac{32}{7}\pi a_{2D}{}^2. \tag{4.3}$$

The correct description of phase-space filling gives essentially the same result as the intuitive hard-core model with, however, an effective excitonic area about twice as large than that defined by its Bohr radius. This again is intuitively easy to understand. The Bohr radius corresponds to the maximum of the relative probability density in the 1S state, i.e., $P(r) = 2\pi r|U(r)|^2$, but, as is seen in Fig. 3, the actual density extends well beyond a circle of radius a_{2D}, and the factor 32/7 simply accounts for that. The band-filling effects that are due to the e–h plasma can be evaluated by the same method but using this time the temperature-dependent Boltzmann distributions. For a binding energy of 9 meV, it is found that the saturation density for free-carrier phase-space filling is approximately 1.5 times smaller than that resulting from excitons.[76] In order to compare the magnitude of the theoretical saturation density with the experimental cross section, we can use Eq. (4.3) to evaluate the exciton Bohr radius. One finds $a_{2D} = 55$ Å, in surprisingly good agreement with the value $a_{2D} = 64$ Å calculated variationally to account for the finite well thickness (see Section 2) in our sample.[36,37]

Let us now discuss the consequences of screening. They are difficult to evaluate in a closed form, especially in the case of our samples that consist of multiple layers of finite thickness. When the screened Coulomb potential is used in the exciton Schrödinger equation, the binding energy and the absorption strength decrease in a correlated manner, as was stressed by Eq. (2.14). We can thus follow the effects of screening on the binding energy, or, since the metal–insulator transition occurs when the binding energy vanishes, we can use the critical density N_c at the transition as scaling parameter to evaluate the screening strength. For static plasma screening in the Debye limit, a rough estimate, deduced from the simple Mott criterion, gives a $N_c \propto kT$ dependence; this shows that the effects of screening decrease strongly with temperature. Although the Mott criterion may overestimate the reduction of screening, it illustrates well how the thermal kinetic energy that favors uniform distributions competes with the electrostatic force, which tends to concentrate the carriers around the potential sources. Numerical calculations confirm this tendency; they indicate that N_c can increase by 1 order of magnitude from low to room temperature. Various theories show that screening by a gas of excitons is less effective than that of a charged plasma at the same temperature. Only a limited number of theoretical studies have considered the question of screening by different temperatures of carriers and excitons, and among them only Refs. 63 and 64 have reported quantitative results. In this work, it was found that, in three dimensions, when the motion of the exciton center of gravity is included in the theory, screening by a cold exciton gas is larger than that of a warm plasma ($T \sim 100$ K). At present, no theory of exciton screening in quasi-2-D systems is available, but the same trends should apply. It should also be remembered that in reduced-dimensionality systems, the contribution of screening to exciton bleaching is considerably decreased compared with that due to phase-space filling.

Therefore we interpret the femtosecond dynamics of the exciton absorption under resonant pumping as resulting from the combination of the large difference between the temperature of the exciton gas and that of the e–h plasma generated by thermal ionization and to the reduction of the strength of screening effects in reduced-dimensionality systems.

Of course, the experimental comparison of the relative consequences of low-temperature excitons versus a warm plasma is difficult to perform accurately in a bulk crystal. Our experiment has the unique ability to compare directly the

effects of the two species at precisely the same density. Our investigation has shown a most unusual optical nonlinearity that comprises two contributions; one contribution has a fast recovery time and also has a nonlinear cross section about twice as large as the second contribution that recovers much more slowly. The practical consequences of nonlinearities of this type have not yet been fully investigated, although there is some speculation that they might be involved in the pulse-shaping mechanisms of laser-diode mode locking[77] using a MQWS saturable absorber.

5. CONCLUSIONS

Excitonic effects in ultrathin semiconductor layers are strongly modified by quantum-size effects. The confinement in a layer whose thickness is smaller than the Bohr radius of the bulk compound increases e–h correlation in MQWS's. This results in a larger binding energy and an enhanced excitonic-absorption strength. A consequence of these effects that is of central interest for the investigations reported in this paper is the observation of exciton resonances at room temperature. Although the resonances are clearly resolved in the absorption spectra, the excitons themselves are unstable against thermal ionization by LO phonons. They release free electrons and holes in about 0.3 psec. Both the existence of the resonances and the rapid ionization of the excitons are important in understanding the nonlinear optical properties of MQWS's near the band gap.

The nonlinear-optical effects in the vicinity of the band gap of MQWS's involve different mechanisms according to the wavelength *and the duration* of the excitation. The same effects are observed either when carriers are directly generated by photoexcitation above the exciton resonances or when optical pulses that are long compared with the exciton ionization time are used. Very efficient nonlinear absorption and refraction are measured. These phenomena are well described by plasma screening and phase-space filling by free carriers. They are large enough to be utilized in device applications, and demonstrations of cw laser-diode four-wave mixing, generation of picosecond pulses by laser-diode mode locking, and optical bistability have already been reported. In contrast, the nonlinear optical processes induced by ultrashort pulses depend critically on the wavelength of excitation. When ultrashort optical pulses with photon energy centered at the exciton-peak transition are used to create excitons selectively, it is possible to time-resolve the effects of the bound e–h pairs on the absorption spectrum and to follow their ionization in real time. The modifications of the absorption observed after ionization are same as those seen with long pulses or with nonresonant ultrashort excitations. However, at very short times, a strong bleaching of the exciton peak occurs; unexpectedly, the nonlinear optical effects that are due to the gas of neutral bound pairs are found to be approximately *twice as efficient* as those induced by free-e–h pairs. The explanation of these large effects with an exciton gas is phase-space filling by the excitons, which directly blocks the creation of further excitons. These effects can be larger than the effects resulting from the warm free carriers because (1) the effective temperature of the carrier distribution that corresponds to the exciton is low (at least before the exciton interacts with the phonons), and so phase-space filling and exchange effects are relatively strong, and (2) the screening by free carriers is weakened by the high temperature of the carriers and by the reduced dimensionality.

Nonlinear-optical effects associated with changes of population are usually thought to be slow because they are normally controlled by the population relaxation time to the ground state or to states of lower energy. The unusual nature of the relaxation of excitons in MQWS's at room temperature introduces a new concept in nonlinear optics. This system has the peculiarity of relaxing at least initially toward states of *higher energy and of larger temperature.* In such systems, it becomes possible to create a cold population that is efficient in changing the optical properties and that transforms in a subpicosecond time into another, longer-lived species. Because the final species is half as efficient as the initial one in changing some of the optical properties of the material, large and yet fast nonlinearities are obtained. The consequences of these features have not yet been completely explored; they may already be playing an important role in laser-diode mode locking.

ACKNOWLEDGMENTS

The research presented in this article was performed at AT&T Bell Laboratories in collaboration with W. H. Knox, J. S. Weiner, M. C. Downer, P. W. Smith, D. J. Eilenberger, R. L. Fork, and C. V. Shank. The samples were expertly grown by A. C. Gossard, A. Y. Cho, W. Wiegmann, and D. Sivco. We also wish to acknowledge several stimulating discussions with S. Schmitt-Rink and H. Haug.

REFERENCES

1. See, for example, E. I. Rashba and M. D. Sturge, eds., *Excitons*, Vol. 2 of Modern Problems in Condensed Matter Science (North-Holland, Amsterdam, 1982).
2. See, for example, R. Dingle, ed. *Device and Circuit Applications of III–V Semiconductor Superlattice and Modulation Doping* (Academic, New York, 1985).
3. See, for example, L. L. Chang and K. Ploog, eds., *Molecular Beam Epitaxy and Heterostructures*, (Nijhoff, Dordrecht, The Netherlands, 1985).
4. R. Dingle, W. Wiegmann, and C. H. Henry, "Quantum states of confined carriers in very thin AlGaAs–GaAs heterostructures," Phys. Rev. Lett. **33,** 827–830 (1974).
5. J. E. Zucker, A. Pinczuk, D. S. Chemla, A. C. Gossard, and W. Wiegmann, "Delocalized excitons in semiconductor heterostructures," Phys. Rev. B **29,** 7065–7068 (1984).
6. L. I. Shiff, *Quantum Mechanics* (McGraw-Hill, New York, 1955).
7. G. Bastard, "Theoretical investigations of superlattice band structure in the envelope-function approximation," Phys. Rev. B **25,** 7584–7597 (1982).
8. G. Bastard, "Quantum size effects in the continuum states of semiconductor quantum wells," Phys. Rev. B **30,** 3547–3549 (1984).
9. R. C. Miller, A. C. Gossard, D. A. Kleinman, and O. Munteanu, "Parabolic quantum wells with the GaAs–AlGaAs system," Phys. Rev. B **29,** 3740–3743 (1984).
10. R. C. Miller, D. A. Kleinman, and A. C. Gossard, "Energy-gap discontinuities and effective masses for GaAs–AlGaAs quantum wells," Phys. Rev. B **29,** 7085–7087 (1984).
11. R. People, K. W. Wecht, K. Alavi, and A. Y. Cho, "Measurement of the conduction band discontinuity of molecular beam epitaxial grown InAlAs–InGaAs N–n heterojunction by C–V profiling," Appl. Phys. Lett. **43,** 118–120 (1983).
12. J. S. Weiner, D. S. Chemla, D. A. B. Miller, T. H. Wood, D. Sivco,

and A. Y. Cho, "Room temperature excitons in 1.6-μm band-gap GaInAs–AlInAs quantum wells," Appl. Phys. Lett. **46,** 619–621 (1985).
13. J. H. Luttinger and W. Kohn, "Motion of electrons and holes in perturbed periodic fields," Phys. Rev. **97,** 869–883 (1955).
14. G. Dresselhaus, A. F. Kip, and C. Kittel, "Cyclotron resonance of electrons and holes in silicon and germanium crystals," Phys. Rev. **98,** 368–384 (1955).
15. C. Weisbuch, R. C. Miller, R. Dingler, and A. C. Gossard, "Intrinsic radiative recombination from quantum states in GaAs–AlGaAs multi-quantum well structures," Solid State Commun. **37,** 219–222 (1981).
16. R. C. Miller, D. A. Kleinman, W. A. Norland, and A. C. Gossard, "Luminescence studies of optically pumped quantum wells in GaAs–AlGaAs multilayer structures," Phys. Rev. B **22,** 863–871 (1980).
17. U. Ekenberg and M. Altarelli, "Calculation of hole subband at the GaAs–AlGaAs interface," Phys. Rev. B **30,** 3569–3572 (1984).
18. A. Fasolino and M. Altarelli, "Subband structure and Landau levels in heterostructures," in *Heterostructures and Two Dimensional Electron Systems in Semiconductors* (Mauendorf, Austria, 1984).
19. W. T. Tsang, C. Weisbuch, R. C. Miller, and R. Dingle, "Current injection GaAs–AlGaAs multi-quantum well heterostructures lasers prepared by molecular beam epitaxy," Appl. Phys. Lett. **35,** 673 (1979).
20. H. Holonyak, Jr., R. M. Kolbas, W. D. Liadig, B. A. Vojak, K. Hess, R. D. Dupuis, and P. D. Dapkus, "Phonon assisted recombination and stimulated emission in quantum well AlGaAs–GaAs heterostructures," J. Appl. Phys. **51,** 1328–1337 (1980).
21. H. Kobayashi, H. Iwamura, T. Saku, and K. Otsuka, "Polarization-dependent gain-current relationships in GaAs–AlGaAs multi-quantum well laser diodes," Electron. Lett. **19,** 166–167 (1983).
22. M. Asada, A. Kemeyama, and Y. Suematsu, "Gain and intervalence band absorption in quantum well lasers," IEEE J. Quantum Electron **QE-20,** 745–753 (1984).
23. M. Yamanishi and I. Suemune, "Comments on polarization dependent momentum matrix elements in quantum well lasers," Jpn. J. Appl. Phys. **23,** L35–36 (1984).
24. M. Yamada, S. Ogita, M. Yamanishi, K. Tabata, N. Nakaya, M. Asada, and Y. Suematsu, "Polarization-dependent gain in GaAs–AlGaAs multi-quantum well laser: theory and experiments," Appl. Phys. Lett. **45,** 324–325 (1984).
25. R. Sooryakumar, D. S. Chemla, A. Pinczuk, A. Gossard, W. Wiegmann, and L. Sham, "Band mixing in GaAs–AlGaAs heterostructures," Solid State Commun. (to be published).
26. R. J. Elliott, "Intensity of optical absorption by excitons," Phys. Rev. **106,** 1384–1389 (1957).
27. J. D. Dow and D. Redfield, "Electroabsorption in semiconductors: the excitonic absorption edge," Phys. Rev. B **1,** 3358–3371 (1970).
28. L. V. Keldysh, "Coulomb interaction in thin semiconductor and semimetal films," JETP Lett. **29,** 658–661 (1979).
29. M. Shinada and S. Sugano, "Interband optical transitions in extremely anisotropic semiconductors. I: Bound and unbound exciton absorption," J. Phys. Soc. Jpn. **21,** 1936–1946 (1966).
30. Y. C. Lee and D. L. Lin, "Wannier excitons in thin crystal films," Phys. Rev. B **19,** 1982–1989 (1979).
31. T. F. Jiang, "An alternative approach to exciton binding energy in GaAs–AlGaAs quantum wells," Solid State Commun. **50,** 589–593 (1984).
32. R. C. Miller, D. A. Kleinman, W. T. Tsang, and A. C. Gossard, "Observation of excited levels of excitons in GaAs quantum wells," Phys. Rev. B. **24,** 1134–1136 (1981).
33. G. Bastard, E. E. Mendez, L. L. Chang, and L. Ezaki, "Exciton binding energy in quantum wells," Phys. Rev. B **26,** 1974–1979 (1982).
34. R. L. Greene and K. K. Bajaj, "Binding energy of Wannier excitons in GaAs–AlGaAs quantum well structures," Solid State Commun. **45,** 831–835 (1983).
35. R. L. Greene, K. K. Bajaj, and D. E. Phelps, "Energy levels of Wannier excitons in GaAs–AlGaAs quantum well structures," Phys. Rev. B **29,** 1807–1812 (1984).
36. D. A. B. Miller, D. S. Chemla, T. C. Damen, A. C. Gossard, W. Wiegmann, T. H. Wood, and C. A. Burrus, "Bandedge electroabsorption in quantum well structures: the quantum confined Stark effect," Phys. Rev. Lett. **53,** 2173–2177 (1984).
37. D. A. B. Miller, D. S. Chemla, T. C. Damen, A. C. Gossard, W. Wiegmann, T. H. Wood, and C. A. Burrus, "Electric field dependence of optical absorption near the bandgap of quantum well structures," Phys. Rev. B (to be published).
38. C. Weisbuch, R. Dingle, A. C. Gossard, and W. Wiegmann, "Optical characterization of interface disorder in multi-quantum well GaAs–AlGaAs superlattice structures," J. Vac. Sci. Technol. **17,** 1128–1129 (1980).
39. See, for example, J. Hegarty and M. D. Sturge, "Studies of exciton localization in quantum-well structures by nonlinear-optical techniques," J. Opt. Soc. Am. B **2,** 1143–1154 (1985).
40. J. C. Maan, G. Bell, A. Fasolino, M. Altarelli, and K. Ploog, "Magneto-optical determination of exciton binding energy in GaAs–AlGaAs quantum well structures," Phys. Rev. B **30,** 2253–2256 (1984).
41. J. E. Zucker, A. Pinczuk, D. S. Chemla, A. C. Gossard, and W. Wiegmann, "Raman scattering resonant with quasi two dimensional excitons in semiconductor quantum wells," Phys. Rev. Lett. **51,** 1293–1196 (1983).
42. J. E. Zucker, A. Pinczuk, D. S. Chemla, A. C. Gossard, and W. Wiegmann, "Optical vibrational modes and electron-phonon interaction in GaAs quantum wells," Phys. Rev. Lett. **53,** 1280–1283 (1984).
43. D. A. B. Miller, D. S. Chemla, P. W. Smith, A. C. Gossard, and W. T. Tsang, "Room temperature saturation characteristics in GaAs–AlGaAs multiple quantum well structures and of bulk GaAs," Appl. Phys. B **28,** 96–97 (1982).
44. T. Ishibashi, S. Tarucha, and H. Okamoto, "Excitons associated optical absorption spectra of AlAs/GaAs superlattices at 300 K," AIP Conf. Proc. **63,** 587–588 (1981).
45. S. W. Kirchoefer, N. Holonyak, K. Hess, D. A. Gulino, H. G. Drickamer, J. J. Coleman, and P. D. Dapkus, "Absorption measurements at high pressure on AlAs–AlGaAs–GaAs superlattices," Appl. Phys. Lett. **40,** 821–824 (1982).
46. J. S. Weiner, D. S. Chemla, D. A. B. Miller, H. Haus, A. C. Gossard, W. Wiegmann, and C. A. Burrus, "Highly anisotropic properties of single quantum well wave guides," Appl. Phys. Lett. (to be published).
47. D. A. B. Miller, D. S. Chemla, P. W. Smith, A. C. Gossard, and W. T. Tsang, "Large room temperature optical nonlinearily in AlGaAs–GaAs multiple quantum well structures," Appl. Phys. Lett. **41,** 679–681 (1982).
48. D. S. Chemla, D. A. B. Miller, P. W. Smith, A. C. Gossard, and W. Wiegmann, "Room temperature excitonic nonlinear absorption and refraction in GaAs–AlGaAs multiple quantum well structures," IEEE J. Quantum Electron. **QE-20,** 265–275 (1984).
49. V. I. Alperowich, V. M. Zal, A. F. Kranchinko, and A. S. Terekhev, "The influence of phonons and impurities on the broadening of excitonic spectra in gallium arsenide," Phys. Status Solidi **b77,** 466–471 (1976).
50. N. F. Mott, *Metal-Insulator Transitions* (Taylor & Francis, London, 1974).
51. H. Haug and S. Schmitt-Rink, "Electron theory of optical properties of laser excited semiconductors," Prog. Quantum Electron. **9,** 3–100 (1984).
52. H. Haug and S. Schmitt-Rink, "Basic mechanisms of the optical nonlinearities of semiconductors near the band edge," J. Opt. Soc. Am. B **2,** 1135–1142 (1985).
53. S. Schmitt-Rink, C. Ell, and H. Haug, "Excitons and electron hole plasma in quasi two dimensional systems," in *Proceedings of the Third IUPAP Semiconductor Symposium* (North-Holland, Amsterdam, 1985).
54. D. Pines and P. Nozieres, *The Theory of Quantum Liquids* (Benjamin, New York, 1966).
55. J. Lindhard, "On the properties of a gas of charge particles," K. Dan. Vidensk. Selsk. Mat. Fys. Medd. **28,** 8–57 (1954).
56. B. I. Lundquist, "Single particle spectrum of the degenerate electron gas," Phys. Condens. Matter **6,** 193 (1967).
57. T. M. Rice, "Quasi-particle properties in an electron-hole liquid," Nuovo Cimento Soc. Ital. Fis. B **23,** 226–233 (1974).
58. R. Zimmermann and M. Rosler, "Theory of electron hole plasma in CdS," Phys. Status Solidi **75,** 633–645 (1976).
59. P. Vashista and R. K. Kalia, "Universal behaviour of exchange–

correlation energy in electron hole liquids," Phys. Rev. B **25**, 6492–6495 (1982).
60. J. D. Dow, "Excitons in degenerate and nondegenerate semiconductors," in *Proceedings of the Twelfth International Conference on Semiconductor Physics* (Teubner, Stuttgart, 1974), pp. 957–961.
61. G. W. Ferhrenbach, W. Shafer, J. Treusch, and R. G. Ulbrich, "Transient spectra of dense exciton gas in a direct gap semiconductor," Phys. Rev. Lett. **49**, 1281–1284 (1982).
62. J. P. Vinti, "Relation between electric and diamagnetic susceptibilities of monoatomic gases," Phys. Rev. **41**, 813–817 (1932).
63. J. H. Collet and T. Amand, "Electron hole interaction in the presence of excitons," Solid State Commun. **52**, 53–56 (1984).
64. J. H. Collet, "Exciton plasma transition in GaAs," J. Phys. Chem. Solids (to be published).
65. D. A. B. Miller, D. S. Chemla, D. J. Eilenberger, P. W. Smith, A. C. Gossard, and W. Wiegmann, "Degenerate four wave mixing in room temperature GaAs–AlGaAs multiple quantum well structures," Appl. Phys. Lett. **42**, 925–927 (1983).
66. J. S. Weiner, D. S. Chemla, D. A. B. Miller, D. Pearson, D. Sivco, and A. Y. Cho, "Nonlinear optical properties of GaInAs–AlInAs quantum well structures," Appl. Phys. Lett. (to be published).
67. P. W. Smith, Y. Silberberg, and D. A. B. Miller, "Mode locking of semiconductor diode lasers using saturable excitonic nonlinearities," J. Opt. Soc. Am. B **2**, 1228–1236 (1985).
68. N. Peyghambariam and H. M. Gibbs, "Optical nonlinearity, bistability, and signal processing in semiconductors," J. Opt. Soc. Am. B **2**, 1215–1227 (1985).
69. C. V. Shank, "Measurement of ultrafast phenomena in the femtosecond time domain," Science **219**, 1027–1031 (1983).
70. W. H. Knox, R. F. Fork, M. C. Downer, D. A. B. Miller, D. S. Chemla, and C. V. Shank, "Femosecond dynamics of nonequilibrium correlated electron-hole pairs distribution in room temperature GaAs multiple quantum well structures," in *Ultrafast Phenomena IV*, D. H. Auston and K. B. Eisenthal, eds. (Springer-Verlag, Berlin, 1984), pp. 162–165.
71. W. H. Knox, R. F. Fork, M. C. Downer, D. A. B. Miller, D. S. Chemla, and C. V. Shank, "Femtosecond dynamics of resonantly excited excitons in room temperature GaAs quantum wells," Phys. Rev. Lett. **54**, 1306–1309 (1985).
72. C. V. Shank, R. L. Fork, R. Yen, and C. A. Hirlimann, "Femtosecond optical pulses," IEEE J. Quantum Electron. **QE-19**, 500–506 (1983).
73. E. M. Conwell and M. O. Vassell, "High field distribution function in GaAs," IEEE Trans. Electron. Dev. **ED-13**, 22–27 (1966).
74. T. Ando, A. Fowler, and F. Stern, "Electronic properties of two dimensional systems," Rev. Mod. Phys. **54**, 437–672 (1982).
75. A. L. Fetter, "Electro dynamics of a layer electron gas. II. Periodic array," Ann. Phys. **88**, 1–25 (1982).
76. S. Schmitt-Rink, D. S. Chemla, and D. A. B. Miller, "Theory of dynamics of room temperature excitonic nonlinearities in semiconductor quantum well," Phys. Rev. B (to be published).
77. H. A. Haus and Y. Silberberg, "Theory of mode locking of a laser diode with a multiple-quantum-well structure," J. Opt. Soc. Am. B **2**, 1237–1243 (1985).

D. S. Chemla

D. S. Chemla was born in Tunis, Tunisia, on July 21, 1940. He graduated from the École Nationale Supérieure des Télécommunications, Paris, in 1965. He received the *Doctorat Es-Sciences* from the Faculty of Sciences of Paris in 1972. From 1965 to 1967, he worked at the Collège de France in high-energy physics. From 1967 to 1981, he worked at the Centre National d'Études des Télécommunications as an MTS Group Leader and department head. He joined AT&T Bell Laboratories, Holmdel, New Jersey, in 1981 and is now the head of the Quantum Physics and Electronic Research Department. He has been engaged in research on nonlinear optics of insulators, organic molecules and crystals, and semiconductors. He is currently interested in the optical response of microstructures under excitation by ultrashort and high-intensity light pulses.

D. A. B. Miller

D. A. B. Miller was born in Hamilton, U.K., in 1954. He received the B.Sc. degree in physics from St. Andrews University, U.K., in 1976, and the Ph.D. degree from Heriot-Watt University, Edinburgh, U.K., in 1979. He remained at Heriot-Watt University until 1981, latterly as a lecturer in the Department of Physics, where he worked on nonlinear optics of semiconductors and optical bistability. Since 1981, he has been a member of technical staff in the Laser Science Research Department at AT&T Bell Laboratories. His current research interests include the physics and applications of nonlinear optics and electro-optics in semiconductor quantum-well material.